LncRNA *RUS* shapes the gene expression program towards neurogenesis

Marius F. Schneider[1,2,] Veronika Müller[2], Stephan A. Müller[3,4], Stefan F. Lichtenthaler[3,4,5], Peter B. Becker[1]* and Johanna C. Scheuermann[2]

[1] Division of Molecular Biology and [2] Division of Metabolic Biochemistry, Biomedical Center Munich, Ludwig-Maximilians-University, Munich, Germany.

[2] Division of Metabolic Biochemistry, Faculty of Medicine, Biomedical Center (BMC), Ludwig-Maximilians-Universität München, Munich, Germany

[3]Neuroproteomics, School of Medicine, Klinikum rechts der Isar, Technical University of Munich, 81675 Munich, Germany

[4] German Center for Neurodegenerative Diseases (DZNE) Munich and Neuroproteomics Unit, Technical University, Munich.

[5] Munich Cluster for Systems Neurology (SyNergy), Munich, Germany

*To whom correspondence should be addressed:

Peter B. Becker
Biomedical Center, Division of Molecular Biology, LMU Munich
Großhaderner Strasse 9
82152 Planegg-Martinsried, Germany
Tel: +49 89 2180 75427
Email: pbecker@bmc.med.lmu.de

Abstract

The evolution of brain complexity correlates with an increased expression of long, non-coding (lnc) RNAs in neural tissues. Although prominent examples illustrate the potential of lncRNAs to scaffold and target epigenetic regulators to chromatin loci, only few cases have been described to function during brain development.

We present a first functional characterization of the lncRNA *LINC01322*, which we term RUS for 'RNA upstream of Slitrk3'. The *RUS* gene is well conserved in mammals by sequence and synteny next to the neurodevelopmental gene Slitrk3. *RUS* is exclusively expressed in neural cells and its expression increases along with neuronal markers during neuronal differentiation of mouse embryonic cortical neural stem cells. Depletion of *RUS* locks neuronal precursors in an intermediate state towards neuronal differentiation resulting in arrested cell cycle and increased apoptosis. *RUS* associates with chromatin in the vicinity of genes involved in neurogenesis, most of which change their expression upon *RUS* depletion. The identification of a range of epigenetic regulators as specific *RUS* interactors suggests that the lncRNA may mediate gene activation and repression in a highly context-dependent manner.

Keywords

chromatin / lncRNA / Gm20754 / neurogenesis / ChIRP-seq

Introduction

Most parts of a higher eukaryotic genome are transcribed at times and in certain cells, but only a minority of the resulting RNAs are protein-coding. While many of these non-coding transcripts are immediately degraded, others are processed into small RNAs that form an intricate network regulating gene expression in a co- and post-transcriptional manner. In addition, mammalian genomes encode thousands of stable RNAs longer than 200 nucleotides, often capped and polyadenylated, but without any obvious coding potential [long, noncoding (lnc) RNAs] (Engreitz *et al*, 2016; Quinn & Chang, 2016; Rutenberg-Schoenberg *et al*, 2016; Kopp & Mendell, 2018). The functions of most lncRNAs discovered in large-scale sequencing projects remain to be explored. 'Guilt-by-association' strategies correlate their presence and expression levels with certain cellular states, including disease conditions. Increasingly, interference strategies reveal critical roles for lncRNAs in cellular fates and states (Statello *et al*, 2021; Rinn & Chang, 2020; Lin *et al*, 2014).

Apparently, lncRNAs arise by pervasive transcription of the genome and evolve fast. Conceivably, their structural flexibility makes them an ideal substrate for 'constructive neural evolution' and predisposes them for a function in chromatin regulation (Palazzo & Koonin, 2020; Rinn & Chang, 2020). Indeed, more than 60% of annotated lncRNAs in human cells are chromatin-enriched (Rinn & Chang, 2012).

In the chromatin context, lncRNAs often combine two functions: scaffolding and targeting. The intrinsic ability of lncRNAs to mediate positional targeting in the genome qualifies them to impose allele-specific epigenetic regulation, such as genome imprinting, X chromosome inactivation or rDNA regulation (Yao *et al*, 2019; Rinn & Chang, 2020; Statello *et al*, 2021). Their actions may be locally restricted close to their site of transcription in *cis*, or in *trans* via sequence-specific hybridization with DNA or RNA. Thus, they may guide powerful 'epigenetic' regulators (enzymes that modify histones or DNA) to specific loci in chromatin, or participate in nuclear condensates (Rutenberg-Schoenberg *et al*, 2016; Kopp & Mendell, 2018; Statello *et al*, 2021; Engreitz *et al*, 2016). Prominent examples of lncRNAs recruiting regulators that define epigenetic chromatin states, include *XIST*, *HOTAIR* and *ANRIL* that bind polycomb complexes (PRC) to silence chromosomal regions, while others such as HOTTIP or certain enhancer RNAs are known to recruit activating histone acetyltransferase or methylase complexes (Werner & Ruthenburg, 2015; Quinn & Chang, 2016).

The fraction of lncRNAs that are expressed in a tissue-specific manner exceeds that of cell type-specific protein-coding genes (Djebali *et al*, 2012). A particular rich compendium of lncRNAs is expressed in the mammalian brain (estimated 40% of known lncRNAs) (Mercer *et al*, 2010; Hezroni *et al*, 2019; Briggs *et al*, 2015), and a strong correlation between the number of expressed lncRNAs and mammalian brain size was reported (Clark & Blackshaw, 2017). Brain-specific lncRNAs tend to be more evolutionary conserved between orthologues than lncRNAs expressed in other tissues and their genes often reside next to protein-coding genes involved in neuronal development or brain function processes (Ponjavic *et al*, 2009). Indeed, lncRNAs are drivers of key neurodevelopmental processes such as neuroectodermal lineage commitment, proliferation of neural precursor cells, specification of the precursor cells, and the differentiation of precursor cells into neurons (neurogenesis) or other neural cell types (gliogenesis) (Briggs *et al*, 2015; Zimmer-Bensch, 2019).

Diverse mechanisms have been documented. For example, lncRNA *TUNA* (*megamind*) is involved in neural differentiation of mouse embryonic stem cells (mESCs) (Lin *et al*, 2014). The finding that depletion of *TUNA* also compromised ESC proliferation and maintenance of pluripotency illustrates the power of lncRNA to control gene networks in diverse ways,

depending on the nature of protein effectors and the timing and context of their lncRNA interactions (Lin *et al*, 2014). The lncRNA *RMST* promotes neuronal differentiation by recruiting the transcription factor Sox2 to promoters of neurogenic genes (Ng *et al*, 2013). The lncRNA *Pinky* is expressed in the neural lineage, where it helps to maintain the proliferation of a transit-amplifying cell population, thereby restraining neurogenesis. This regulation takes place at the level of transcipt splicing, illustrating the versatility of nuclear lncRNAs (Ramos *et al*, 2015). Other mechanisms involve the control of miRNA availability and function, as has been shown for the primate-specific lncND during neurodevelopment (Rani *et al*, 2016).

Only a small fraction of lncRNAs involved in neurodevelopment and brain function has been studied in detail. We here describe a novel lncRNA involved in neurogenesis, which we term *RUS* (for 'RNA upstream of Slitrk3'). The *RUS* gene resides at a syntenic position in mouse and human genomes upstream of the Slitrk3 gene, which encodes a transmembrane protein involved in suppressing neurite outgrowth. *RUS* is expressed in neural tissues only and its expression increases during the differentiation of neural stem cells into neurons. *RUS* is a nuclear lncRNA that interacts with chromatin in the vicinity of genes involved in neurogenesis. Depletion of RUS results in massive alterations in the gene expression program of neuronal progenitor cells, trapping them in an intermediate state during differentiation and eventually leading to proliferation arrest. Proteomic identification of *RUS*-interacting proteins suggests multiple mechanisms of *RUS*-mediated epigenetic gene regulation.

Results

Identification of the neuronal-specific lncRNA RUS

To identify novel, functionally relevant lncRNAs in the context of neurogenesis, we searched for transcripts lacking obvious coding potential meeting the following criteria. They should 1) only be expressed in neural tissues, 2) be dynamically regulated during the differentiation of neural precursor cells and 3) be conserved between mouse and humans (Fig 1A). We examined the expression of 553 candidate lncRNAs in human ESC-derived neural progenitor cells: neuroepithelial cells (NE), early, mid and late radial glia cells (ERG, MRG, LRG, respectively) before and after differentiation (Ziller *et al*, 2015). Of these, 10 transcripts decrease and 29 increase during the differentiation of the four cell types (Fig 1B). Among them, we identified *LINC01322* as an interesting candidate, as it was absent in NE, ERG and MRG, but expressed in all differentiated cell types. Intriguingly, *LINC01322* was also expressed in undifferentiated LRG.

LncRNA genes relevant to neurogenesis are often located next to neurodevelopmental protein-coding genes (Ponjavic *et al*, 2009). In line with this observation, the gene for *LINC01322* localizes upstream of the gene encoding the transmembrane protein Slitrk3, which regulates neurite outgrowth (Aruga *et al*, 2003) (Fig 1C). In the following, we refer to *LINC01322* as *RUS* (*RNA upstream to Slitrk3*). The location of the *RUS* gene is well conserved by synteny in mice and humans between the *Slitrk3* and *Bche-201* genes (Fig 1C).

The murine *RUS* transcript, *Gm20754,* has two annotated isoforms. Two and five exons are annotated for isoforms 1 and 2, respectively. Both isoforms share the 232 bp exon 1, which is 75% similar to the orthologous counterpart in humans (Fig 1C). The sequence of *mRUS* exon 2 (114 bp) is conserved to 92%, but not part of the predominant human transcript. I*n silico* open reading frame (ORF) predictions revealed that the largest ORF encodes a

theoretical polypeptide of 80 amino acids (aa). Since the corresponding peptides are not listed in published mass spec data (PeptideAtlas), we assume that *RUS* functions as a lncRNA.

Quantitative RT-PCR analysis of the two isoforms in different mouse adult and embryonic tissues revealed that *RUS* annotated isoform 1 is the dominant form (Fig 1D). *RUS* expression is restricted to neural tissues, with highest expression in the adult hippocampus. Continuing with isoform 1, we performed 3'-RACE experiments to obtain the annotated 3' end (Fig EV1A). However, amplification of *RUS* with primers targeting the annotated 5' and 3' ends yielded two PCR bands of 1.3 kbp and 0.9 kbp. Sequencing the more abundant 0.9 kbp PCR band revealed that it lacked exon 4. (Fig EV1B).

RUS depletion leads to reduced neuronal differentiation, proliferation arrest and increased apoptosis.

To monitor the expression of *RUS* during murine neurogenesis, we differentiated embryonic cortical neural stem cells (NSC) into immature neurons *in vitro* (Kilpatrick & Bartlett, 1993; Azari *et al*, 2011; Mukhtar *et al*, 2020). Differentiating NSC were maintained proliferative by mitogen (bFGF) for the first 4 days. On day 5, bFGF was withdrawn to induce neurogenesis (Fig EV2A). During a time course of 9 days the expected changes in molecular marker expression were detected via immunostaining and quantitative RT-PCR (RT-qPCR) analyses. The high expression of the NSC marker nestin decreased, with a concomitant increase in RGC markers Gfap, Glast and GluL (Fig 2A, EV2A,B), as observed elsewhere (Imura *et al*, 2003; Mamber *et al*, 2012). Upon bFGF withdrawal, the culture acquired neuronal features with high expression of the neuronal markers Map2, Dcx, β-tubulin III and Mapt (Fig 2A, EV2A-B). The expression level of *RUS* continually increased along with the neuronal markers, reaching robust expression on day 5 of the differentiation process (Fig 2A, EV2B).

To explore a potential involvement of *RUS* during neuronal differentiation, we depleted *RUS* by RNA interference, expressing a *RUS*-targeting shRNA (shRNA^{RUS}*)* upon lentiviral transduction into differentiating NSC [Fig 2B, Table EV1, (Moffat, et al., 200*6)]. The shRNA*^{RUS} was selected to have no predicted off-targets, while significantly reducing RUS levels. Upon expression of shRNA^{RUS}*, RUS* levels were typically reduced by approximately 50% compared to control cells expressing a scrambled control shRNA^{CON} (Fig 2C). Remarkably, upon *RUS* depletion the number of cells expressing the neuron-specific β-tubulin III or the dendritic marker Map2 were reduced to 37% and 8%, respectively (Fig 2D).

The specificity of the knockdown was assessed by a rescue experiment. *RUS*-depleted and control cells were transduced with lentiviruses expressing *RUS* driven by the strong CMV promoter (Fig 2E). RT-qPCR revealed that *RUS* was increased roughly 20-fold compared to endogenous, wildtype levels (Fig 2F). Immunostaining of the cells for β-tubulin III served as a proxy for neurogenesis (Fig 2G). *RUS* expression in cultures that had been depleted of endogenous RUS largely restored the number of β-tubulin III-positive cells but did not further increase this value in the presence of endogenous *RUS* (Figure 2H).

RUS depletion led to reduced cell numbers in culture, which may be a consequence of reduced cell proliferation or increased apoptosis. To explore whether this cell loss was due to reduced cell proliferation, we supplemented differentiating NSC cultures with BrdU and monitored its incorporation by immunostaining as a measure of replication (Figure EV2C,D). *RUS* depletion reduced the number of BrdU-positive, proliferating cells by 93.7% (Figure EV2D). We also probed for apoptosis. We replaced the puromycin resistance gene in the

shRNA vector by a GFP gene to visualize knockdown cells while avoiding cell death due to puromycin selection (Figure EV2C). Immunostaining for cleaved caspase 3 in GFP-positive cells revealed a 9-fold increase of apoptosis in shRNA^{RUS}-expressing cells compared to a very low level in control cultures (Figure EV2E). We conclude that the depletion of RUS in differentiating NSCs inhibits cell proliferation and induces apoptosis.

Depletion of RUS locks neural progenitor cells in their differentiation stage.

For an in-depth characterization of the shRNA^{RUS} knockdown phenotype in differentiating NSC we monitored transcriptional changes by RNA-seq analysis. We established the transcriptome at days 5 and 7 after seeding, when endogenous RUS expression is drastically increased, in cells either treated with shRNA^{RUS} or shRNA^{CON} (Fig EV3A, Table EV2). RNA interference by shRNA^{RUS} reduced *RUS* levels to roughly 50%, as before (Fig EV3B). Despite this incomplete depletion, the principal component analysis (PCA) of four replicates clearly separated shRNA^{CON} and shRNA^{RUS} transcriptome profiles at both time points (Fig EV3C).

Next, we determined differentially expressed genes (Fig EV3D, Table EV2) and analyzed enriched gene ontology (GO) classifications (Mi *et al*, 2013) among the up- and down-regulated genes, separately for the two time points. Depletion of *RUS* massively affected the transcriptome: on day 5, 4978 genes (24%) were transcribed at elevated levels under reduced *RUS* levels and 4586 genes (22%) were repressed (Fig EV3D). The expression changes were even more profound on day 7, when 6623 genes (30%) and 6456 genes (29%) were up- or downregulated, respectively.

In agreement with the observed increase of apoptosis upon *RUS* depletion, we found the GO annotations associated with 'cell death' and ‘apoptosis’ (represented by ‘positive regulation of apoptosis’ in Fig 3A) enriched among the induced genes on both days 5 and 7, exemplified by genes encoding, Bak1, and Foxo3. Figure 3B shows these genes among the 50 most deregulated genes enriching for the GO annotations: 'cell-death', 'neurogenesis', 'cell-cycle' and 'microtubule-based process'. Annotations represented by GO classifications ‘cell cycle and ‘microtubule-based process’ (Fig 3A) were most significantly enriched among the downregulated genes on both days, in support of the reduced BrdU incorporation (Fig EV2E) and indicative of proliferation arrest (Fig 3A,B). Interestingly, genes with GO annotations relating to 'neurogenesis' and 'neuron differentiation' were mildly enriched among the downregulated on day 5, but strongly enriched among the induced genes on day 7 (Fig 3A,B). Of note, at this level of analysis direct and indirect effects cannot be distinguished.

To explore the effects of *RUS* depletion in our RNA-seq data in more detail, we determined the read counts of several prominent genes that characterize the *in vitro* differentiation process (Fig 3C). We assessed the proliferation state (*Pcna* and *Ki67*), the NSC/RGC markers *Sox2*, *Pax6* and *Gfap* as well as the neuronal markers *Neurog2*, *Neurod1*, *Map2, Camk2a*, *Grin3a*, and *Gabrb1*. In addition, we focused on the Notch1/2 and sonic hedgehog (Shh) signaling pathways regulating the expansion of RGCs and transit-amplifying intermediate progenitor cell populations. *Notch1/2,* its ligand *Dll1* and their downstream effectors *Hes1, Neurog2, and Ascl1* form an oscillatory network that regulates RGC cell renewal (Hatakeyama & Kageyama, 2006; Wang *et al*, 2016; Ivanov, 2019; Sueda & Kageyama, 2019). We also included *Rest* as a transcriptional repressor of neuro-specific genes which helps to maintain the neural stem cell state (Schoenherr & Anderson, 1995; Mukherjee *et al*, 2016).

Our RNA-seq analysis confirmed that the proliferative markers *Pcna* and *Ki67* were robustly downregulated on both day 5 and day 7 (Fig 3C). The NSC/RGC markers *Sox2, Pax6, Gfap* were less affected. However, the substantially reduced expression of the neuronal cell fate commitment markers *Hes1*, and *Shh* as well as of the neuronal markers: *Neurog2*, *Neurod1*, *Camk2a*, *Grin3a*, and *Gabrb1* confirmed our earlier notion that depletion of *RUS* compromises neuronal differentiation. Of note, the expression of those genes that are most strongly induced during neurogenesis between days 5-7 (i.e., *Shh*, *Neurog2*, and *Neurod*) was most strongly affected by *RUS* depletion (Fig 3C). The increased expression of Notch2 is consistent with the observed maintenance of NSC/RGC markers, the reduced expression of cell cycle genes as well as genes involved in neurogenesis (Engler *et al*, 2018; Mase *et al*, 2021). The induction of *Rest* at day 7 suggests a mechanism involving chromatin regulation.

We conclude that *RUS* is required for efficient proliferation and for differentiation of neuronal precursor cells in this *in vitro* system. The concomitant inhibition of cell proliferation (and hence cell renewal) and neurogenic differentiation may leave neuronal progenitor cells with conflicting signals that trigger apoptosis. The observation that at day 7 the most deregulated genes with annotated GO term 'neurogenesis' are activated upon *RUS* depletion (Fig 3B) prompts the speculation that *RUS* may be involved in the repression of transcription. Again, direct and indirect effects cannot be distinguished at this point.

RUS associates with chromatin of key neurodevelopmental genes.

As a first step towards defining the mechanism through which *RUS* regulates gene expression, we determined the subcellular localization of *RUS*. After two days in culture, cells were fractionated into the cytoplasm, nucleoplasm and chromatin. RT-qPCR analyses showed that *RUS* is enriched in the chromatin fraction, similar to the splicing-associated lncRNA *MALAT* (Fig 4A). An RNA-FISH (fluorescence-*in-situ*-hybridization) experiment confirmed the nuclear localization (data not shown).

To explore whether *RUS* localizes to specific chromosomal regions like other regulatory lncRNAs, we applied the ChIRP (Chromatin Isolation by RNA Purification) methodology (Chu *et al*, 2011). Cells were harvested at day 7 of differentiation and *RUS* was isolated by hybridization with two independent probe sets ('odd' and 'even'). The experiment was done in biological triplicate. All three isolations effectively retrieved *RUS* (approximately 30% of input) and strongly enriched *RUS* over control RNAs *TBP mRNA*, *MALAT* and *XIST* (Fig EV4A). Between 157 to 203 peaks were scored in individual experiments, of which 129 (67%, Fig EV4B) overlapped in all three experiments (Table EV3).

Although we considered only peaks enriched by both probe sets, several enriched genomic sites contained sequences with similarity to one of the used oligonucleotide probe sequences. After removing them, 94 high-confidence putative *RUS* binding sites remained for further analysis (for simplicity called '*RUS* binding sites' below). Genomic annotation revealed that 4 of them (4.3%) mapped to promoters, but the majority predominantly localized to intergenic (35.1%) or intronic (28.7%) regions, compatible with long-range regulatory elements. About a third of the locations mapped close to degenerate repetitive elements of various types, such as LINEs (4.2%), SINEs (12.8%), LTR (6.4%) and simple repeats (8.5%) (Fig 4B). Gene ontology analysis of the active genes next to *RUS* binding sites yielded an enrichment of the terms 'forebrain development', 'neurogenesis' and 'generation of neurons'. Among those are the genes encoding the microtubule stabilizing protein Dclk2 and the potassium voltage-gated channel Kcna1 (Fig 4C, two further tracks:

Arid1b and *Bin1* in Fig EV4C). Both genes play a pivotal role in neuron differentiation (Shin *et al*, 2013; Chou *et al*, 2021).

Following the hypothesis that *RUS* binding to chromatin is involved in regulating near-by genes, we determined the expression changes of genes residing next to *RUS* binding sites (referred to as 'putative target genes' henceforth) using the RNA-seq data of *RUS* knockdown samples. Of the 94 putative target genes, 66 were robustly expressed in differentiating NSC (Fig 4D). The number of genes that changed their expression increased from day 5 to day 7 (54% and 77% of genes with altered expression, respectively), in line with the increase of *RUS* expression between days 5 and 7 of differentiation (Table EV3).

Hierarchical clustering of expression separates putative target genes into two distinct clusters (Fig 4D). Cluster I contains genes significantly downregulated on both days, while cluster II represents genes with enhanced expression, predominantly on day 7. The heat map shows several cluster II genes with reduced expression on day 5 after *RUS* depletion. Since *RUS* depletion was less effective on day 5, we calculated the overall correlation of *RUS* expression and its putative target genes (Fig 4D, purple-to-green boxes to the right of heat maps). If we assume direct effects of *RUS* binding on target gene expression, we expect a positive correlation of genes with reduced expression with *RUS* depletion (essentially genes in cluster I) and a negative correlation of genes with enhanced expression upon *RUS* depletion (predominantly cluster II genes on day 7). This is indeed largely the case (Fig 4D). Remarkably, the expression of genes that are repressed on day 5 and activated on day 7, for example *Arid1b*, *App*, and *Kcna1* (Fig EV4D), correlates positively on day 5 and negatively on day 7 with *RUS* expression, in support of a direct effect of RUS on close-by genes. Our results thus suggest that RUS may mediate both, activating and repressive regulation.

RUS interactors suggest epigenetic regulatory mechanisms.

LncRNAs usually elicit their gene regulatory effects through interacting effector proteins. To explore how *RUS* may mediate both, activating and repressive functions, we sought to identify *RUS*-binding proteins. When mouse and human *RUS* sequences are compared, a remarkable degree of conservation of exon 1 stands out (Fig 1C). Because such conservation may be indicative of important functional interactions, we compared interactors of complete *RUS* with a 5'-deleted RNA *(⊿5'-RUS*), lacking exon 1. Both RNAs were tagged with 5 MS2 stem-loop structures at the 3' end, enabling affinity purification via binding to MS2-binding protein (MS2BP) (Johansson *et al*, 1997; Zhou *et al*, 2002; Tsai *et al*, 2011).

Because differentiating NSCs cannot be obtained in sufficient amounts for RNA-affinity purification, we established an RNA-affinity purification protocol using the well-established Neuro2A cell line. *RUS* is normally not expressed in these cells and so our experiment identifies potential protein interactors that are not relevant in these cells. To assure an equivalent expression of both RNAs, we first generated a Neuro2A derivatives by inserting an FRT recombinase site into the genome through lentiviral transduction. These clonal cells were then transfected with FRT-flanked *RUS* expression constructs along with a flipase expression plasmid (Andrews *et al*, 1985; Sauer, 1994; See *et al*, 2002)). Clones containing integrated *RUS* expression cassettes were expanded and analyzed. These clones express comparable levels of either full-length *RUS* or *⊿5'-RUS*.

Lysates of *RUS*- and ∆5'-*RUS*-expressing cells were incubated with recombinant MS2-binding protein (MS2BP), which in turn was tagged with a maltose-binding protein (MBP) (see scheme in Fig 5A). MS2BP-bound RNA was retrieved by absorption of MBP to amylose

beads, captured proteins were eluted with RNAse A treatment and identified by LC-MS, using label-free quantification (LFQ) (Cox & Mann, 2009).

Full-length *RUS* enriched many more proteins in comparison to ∆5'-*RUS* (Fig 5B, Table EV4). While we cannot exclude that this is due to the increased size of the *RUS* RNA, this seems unlikely given the size difference of 912 (*RUS*) versus 679 nucleotides (*∆5'-RUS).* Proteins with a fold-change greater than 2 and a p-value smaller than 0.002 were considered robust and specific binders. Only 9 proteins were purified selectively along with ∆5'-*RUS.* By contrast, 49 proteins were enriched by co-purification with the full-length construct and therefore considered exon 1-specific interactors (Table 1, EV4). Among them, Phb, Phb2, Tor1aip1 and Utp3 were purified exclusively by the full-length *RUS* RNA.

Phb and Phb2 correspond to the prohibitin complex, a mitochondrial regulator with neuroprotective functions and nuclear co-repressor of cell cycle-regulated genes (Koushyar *et al*, 2015).

Further, we find numerous components of the nuclear periphery, most prominently subunits of the nuclear pore complex (Nupl1, Nup37, Nup43, Nup50, Nup54, Nup85 Nup93, Nup98, Nup107, Nup133, and Seh1l orange in Fig 5B) and several constituents of the nuclear lamina: emerin (Emd), lamins A, B1 and B2 (Lmna, Lmnb1, Lmnb2), lamin B receptor (Lbr) as well as the lamin A/B binding protein Tor1aip1 (red in Fig 5B).

Further, *RUS* exon 1 retrieved many nucleolar proteins (Ddx27, Emg1, Mphosph10, Noc2l, Nifk, Rcl1, Rrp9, Rrs1, Tbl3, Utp3, Wdr3, Wdr12 and Wdr43 green in Fig 5B) and some interesting chromatin regulators (e.g. the bromodomain protein Brd2, the chromatin constituent Hmg20a, the nucleosome remodeling ATPase Smarca5, the lysine demethylase subunit Phf2 and the RNA helicase Ddx54).

The finding of robust interaction of *RUS* with nuclear pores and the lamina suggest well-established epigenetic regulatory mechanisms (to be discussed below). Binding of lncRNA *Xist* to Lbr has been suggested to tether the inactive X chromosome to the nuclear envelope, which forms a silent compartment (Chun-Kan *et al*, 2016). To validate the binding between *RUS* and Lbr we returned to our NSC differentiation model. Nuclear extracts were prepared from cells harvested at day 7 of differentiation. Lbr was immunoprecipitated and co-precipitated RNA quantified by RT-qPCR. *RUS* was retrieved 3.7-fold more by comparison to an anti-IgG purification (Fig 5C). Parallel reactions confirmed the selective interaction of Brd2 with *RUS*, while Sox2 served as a control.

In summary, our data support the idea of the long, noncoding RNA *RUS* as a crucial regulator of the neurogenic gene expression program through epigenetic mechanisms.

Discussion

The lncRNA RUS is required to execute the neurogenic program.

Our study presents a first functional characterization of the lncRNA *LINC01322,* which we term *RUS* (for RNA upstream of *Slitrk3*). Like other neurogenic lncRNAs, *RUS* is well conserved in mammals by sequence and synteny next to the neurodevelopmental gene *Slitrk3*. It is predominantly expressed in neural tissues. Although the RNA bears some coding potential, we did not detect any of the theoretically encoded peptides. *RUS* associates with chromatin at specific sites in the vicinity of neurodevelopmental genes and interacts with several proteins involved in epigenetic gene regulation, suggesting that *RUS* acts as lncRNA.

Transcriptome analyses revealed that sh-mediated depletion of *RUS* results in massive gene expression changes. In fact, approximately half of all genes were affected to a certain degree. The responses were equally divided between gene activation and repression and were modulated during the 7 days of differentiation. This finding is interesting, since most lncRNA studied so far either mediate activation or repression (Rinn & Chang, 2020; Statello *et al*, 2021). Although indirect effects cannot be excluded yet, the fact that we found epigenetic activators and repressors bound to *RUS* exon 1 in pulldown experiments, supports the idea that *RUS* may mediate gene activation and repression in a highly context-dependent manner. Conceivably, *RUS* may function through diverse mechanisms, as emerges for the HOTAIR RNA (Price *et al*, 2021).

On day 5 of differentiation, reduced *RUS* levels correlate with reduced expression of many genes involved in neurogenesis and cell cycle, suggesting that the lncRNA promotes target gene expression to enable amplification of intermediate precursor cells and NSC differentiation. This is in line with the observation that *RUS* is expressed in hESC-derived LRGs (Ziller *et al*, 2015).

RUS is most highly expressed in the adult hippocampus, in which neurogenesis still occurs (Eriksson *et al*, 1998). Adult neurogenesis relies on expanding transit-amplifying IPs maintained by *Shh* expression (Antonelli *et al*, 2018) and differentiation by increased *Neurog2* expression (Galichet *et al*, 2008). At day 7 of our differentiation time course, *Shh*, *Neurog2*, and *NeuroD1* are among the most repressed genes upon *RUS* depletion. In addition, we found a reduced expression of several subunits of glutamate and GABA receptors, such as *Grin3a* and *Gabrb1,* which are predominantly expressed in neurons.

We propose that *RUS* depletion locks neuronal precursors in an intermediate state towards neuronal differentiation, with arrested cell cycle. The activation of pro-apoptotic genes may result from perturbed cell identity.

Potential mechanisms of RUS-mediated gene regulation.

Given the diverse and presumably very site-specific effects of *RUS* function, we can only speculate about potential mechanisms. Our stringent ChIRP approach revealed a very consistent set of *RUS* interactions with a limited number of high-confidence chromatin loci. The localisation of binding sites predominantly in introns and intergenic regions argue for long-range regulation. Considering that the RNA is not highly expressed, we speculate that its range of activity may be limited to the genes in the vicinity of tethering sites (Engreitz *et al*, 2016).

Remarkably, most of the genes closest to a *RUS* binding site were expressed in differentiating NSCs and changed their expression state upon *RUS* depletion. For example, *RUS* binds in the genome next to genes essential for cell cycle and neuronal differentiation, such as *Fgf9, Mapre3, and Ppp6c, Arid1b, Dclk2, and Kcna1.* The expression of these critical genes is affected by *RUS* depletion. Furthermore, *RUS* binding sites can be observed in introns of the E3 ubiquitin ligase genes *Itch* and *Fbxl17*. Itch ubiquitinates Notch proteins for degradation to turn off Notch signaling (Chen *et al*, 2021). *Fbxl17* plays a pivotal role in Shh signaling by degrading Sufu to enable the translocation of Sufu-sequestered transcription factors to the nucleus (Raducu *et al*, 2016). Consequently, reduction of both factors after *RUS* depletion resulted in increased Notch signaling and reduced Shh signaling, consistent with our RNA-Seq data. Notch signaling is important for maintaining the active or quiescent neural stem cell state by preventing neuronal differentiation (Sueda & Kageyama, 2019). Shh signaling regulates proliferation of neural precursors (Yao *et al*, 2016). By activating both

genes *RUS* facilitates proliferation and ensures proper differentiation of neural precursor cells.

LncRNA often work by recruiting epigenetic regulators to locally concentrate them at target chromatin (Markaki *et al*, 2021). Our RNA-affinity purification relies on protein-*RUS* interactions formed under physiological conditions in intact cells and purifying complexes under native conditions. Because we wished to identify proteins interacting with the conserved exon 1 of *RUS*, we monitored the differential binding to RNA containing or lacking this sequence. This is a stringent approach, because functionally meaningful proteins may well (and are indeed likely to) bind to the remainder of *RUS* as well, but they are not discussed here (but see Table EV4). In the following, we discuss hypothetical scenarios, in which *RUS* recruits regulatory functions to chromosomal target loci. It is also possible that *RUS* sequesters the factors in competition with other interactors, which would have opposite effects on gene regulation compared to recruitment scenarios (Xi *et al*, 2022).

Among the proteins purified by full length *RUS* only, the prohibitin complex (consisting of Phb and Phb2) stands out. Prohibitin has functions in several cellular compartments, including mitochondria and nuclei (Wang *et al*, 2002; Fusaro *et al*, 2003; Rajalingam & Rudel, 2005; Koushyar *et al*, 2015). Prohibitin has been termed an oncogene, as it promotes proliferation and dedifferentiation in neuroblast cells (MacArthur *et al*, 2019) and a tumour suppressor gene, since it was shown to inhibit the cell cycle by repressing E2F-regulated genes via recruitment of the retinoblastoma protein and histone deacetylases (Wang *et al*, 2002). It is tempting to speculate that tethering the Phb complex to chromatin contributes to inhibition of proliferation and activation of apoptosis.

Strikingly, the RNA pulldown retrieved numerous proteins of the nuclear envelope. We scored 6 constituents of the nuclear lamina, including three types of lamins and lamin B receptor (Lbr). The inner nuclear membrane assembles a well-known repressive compartment to which inactive heterochromatin is tethered. These lamina-associated domains may be constitutive or facultative (van Steensel & Belmont, 2017). Conceivably, *RUS* mediates tethering of genes destined to be silenced to the lamina, where they acquire heterochromatic features. Such a scenario has precedent in the finding that the lncRNA *XIST* promotes X chromosome inactivation in female cells by tethering the target chromosome to the nuclear envelope via Lbr (Chun-Kan *et al*, 2016).

Repressive heterochromatin is also found at the surface of nucleoli (Kind *et al*, 2013; Vertii *et al*, 2019). Remarkably, we found 13 nucleolar proteins enriched specifically by *RUS* exon 1, which further supports the speculation that *RUS* partitions genes into silencing compartments. However, some of the retrieved nucleolar proteins also have nuclear functions. For example, NOC2L (NOC2 Like Nucleolar Associated Transcriptional Repressor, a.k.a. NIR) associates with p53 in the nucleus to repress a subset of p53-target genes, including p21, by inhibition of histone acetylation (Hublitz *et al*, 2005). Interestingly, the exon 1 interactor NIFK (also a nucleolar protein with nuclear functions) also cooperates with p53 to silence the p21 promoter during checkpoint control (Takagi *et al*, 2001). Apparently, *RUS* also contributes to p21 silencing since the gene gained activity upon depletion of the lncRNA. Similarly, the exon-1 interactor Cdk5rap3 activates p53 activity by repressing its degradation by Hdm2 (Wang *et al*, 2006). Such a scenario provides a plausible and testable hypothesis for the observed cell cycle arrest at reduced *RUS* levels.

In addition to constituents of the nuclear lamina, we found 11 nuclear pore components (Nup11, Nup37, Nup43, Nup50, Nup54, Nup85, Nup93, Nup98, Nup107, Nup133 and Seh1l) among the exon 1 interactors. In addition to nuclear transport, the nuclear pore complex

plays an important role in transcriptional regulation and cell identity, apparently by generating a microenvironment that fosters epigenetic regulation of associated genes (Pascual-Garcia & Capelson, 2021). In *Drosophila*, Nup93 is associated with genes repressed by the polycomb complex and is required for efficient repression (Gozalo *et al*, 2020).

By contrast, three nucleoporins bound *RUS* are predominantly associated with transcriptional activation. Nup98 acts as anchor point for enhancer (Pascual-Garcia *et al*, 2017) and activates transcription by recruiting the Wdr82-Set1A/COMPASS complex to regulate H3K4 trimethylation (Franks *et al*, 2017). Similarly, Nup107 and Seh1l activate transcription by assembling transcription factor (TF) complexes at the nuclear pore (Liu *et al*, 2019). It is tempting to speculate that *RUS* may mediate facultative association of gene loci with the nuclear periphery, which would then be subject to regulation of the corresponding microenvironment. This may initially involve an initial transcriptional activation to execute the differentiation programme. The subsequent compartmentalization of chromosomal loci into a repressive environment may serve to terminally silence cell cycle genes in mature neurons.

The exon 1 interactor HMG20A (a.k.a. iBraf) is known to antagonize repressive LSD1-REST complexes. Since LSD1-REST-dependent H3K4 demethylation represses neuronal genes, HMG20A action promotes neuronal differentiation (Ceballos-Chávez *et al*, 2012; Garay *et al*, 2016). The interaction of *RUS* with HMG20A, therefore, likely affects neuronal differentiation, but whether the outcome is positive (through recruitment) or negative (through squelching) remains to be explored. Of note, REST expression increases upon *RUS* depletion, consistent with the observed inhibition of neurogenesis.

In summary, our mapping of putative target genes and *RUS* interactors are compatible with a range of testable, hypothetical and not mutually exclusive scenarios that may explain the observed change in phenotype and gene expression upon *RUS* depletion during differentiation of NSCs. We propose that *RUS* may be involved in several aspects of the neurogenic program in a highly context-dependent manner, including amplification of precursor cells and terminal neuronal differentiation.

Materials and Methods

Cultivation and differentiation of primary neural stem cells

The isolation of cortical embryonic stem cells from E15-E16 murine cortices was approved by the animal welfare committees of LMU and the Bavarian state. Cortices were dissected from pooled mixed-sex embryonic brains, washed 5 times with Hanks Balanced Salt Solution (HBBS) and incubated in 0.5% Trypsin-EDTA for 15 min. Cortices were then washed 5 times with MEM-HS supplemented with L-glutamine, essential amino acids, non-essential amino acids and 10% horse serum. The single cells in suspension were pelleted at 200 g for 5 min, and seeded at a density of 5 x 10^5 cells/ml. Neural stem cells were cultured in DMEM-F12 with 5% FCS, B27 supplement and 20 ng/ml basic fibroblast growth factor (bFGF) on poly-D-lysine-coated culture dishes at 37°C in 5% CO_2 (Kilpatrick & Bartlett, 1993; Johe *et al*, 1996; Azari *et al*, 2011; Mukhtar *et al*, 2020). Every second day, the culture medium was supplemented with 20 ng/ml bFGF. At 95% confluency cells were diluted 1:2. Differentiation was induced in neurobasal medium with B27 supplement/0.25x Glutamax five days after seeding.

For quantitative RT-PCR analysis or RNA-seq experiments, $3x10^5$ NSC were seeded in 2 ml medium on 35 mm dishes. For microscopy experiments, $1.6x10^5$ NSC were seeded in 1 ml medium on 12.8 mm dishes equipped with 12 mm coverslips.

Sh-mediated knockdown experiments were started one day after seeding by addition of 5 µl virus per 35 mm dish or 3 µl KD virus per 12.8 mm dish. To restore *RUS* expression, 10 µl or 6 µl *RUS* overexpression-virus per 35 mm or 12.8 mm dish, respectively, was added to KD cells four days after seeding.

Cultivation of Neuro2A cells.

Neuro2A cells were cultured in DMEM-Glutamax and 10% FCS at 37°C in 5% CO_2.

Immunohistochemistry.

Cells were plated on poly-L-lysine-coated glass plates in a 24-well plate. All cell washes were done in PBS, all incubations were at RT. Cells were fixed in 4% paraformaldehyde (PFA) for 20 min at RT, washed once for 10 min and blocked with blocking solution (0.3% Triton X-100, 2% donkey serum in PBS) for 30 min. The primary antibody (1:1000) was diluted in 200 µl blocking solution and added for 1.5 h while shaking. The antibody solution was removed, and the cells were washed three times for 10 min. Cells were incubated with the secondary antibody (1:2000) in 200 µl blocking solution for 1.5 h as before. After three 10-minute washes nuclei were stained for 15 min using DAPI (2-[4-Amidinophenyl]-6-indolecarbamidine dihydrochloride,) 1:1000 in PBS. The cells were mounted in the presence of diazabicyclo-octane (DABCO). Stained cells were analyzed with a Leica DM8000 fluorescent microscope, and images were quantitatively processed with ImageJ. Images from DAPI and antibody staining were thresholded, colocalized and watershed-transformed. The particles in the resulting overlay image were counted using the particle analyzer. Per experiment, 3-5 microscope fields on 3-4 plates each were recorded and analyzed.

BrdU-labeling.

Cull culture medium was supplemented with 1 µg/ml bromodesoxyuridine. After 24 hours, cells were immunostained with an anti-BrdU antibody.

Quantitative reverse transcription-PCR (RT-qPCR).

RNA from cells, tissues or biochemical experiments was extracted with Trizol and chloroform and precipitated using 50% isopropanol and 15 µg linear acrylamide. RNA was washed twice with 75% EtOH, dissolved in nuclease-free water and reverse-transcribed using MMuLV RT (Thermo Fischer) and oligo(dT18-20). ChIRP and RIP-purified RNA was amplified with random hexamers. Quantitative RT-PCR analysis was performed with 1 µM of each primer in Fast SYBR® Green Master Mix (Thermo Fischer). The ΔCt values were normalized with amplicons detecting against TATA-binding protein (TBP) mRNA.

3′ RACE.

The RUS 3'-end was cloned from a hippocampal RNA using the FirstChoice™ RLM-RACE Kit (Thermo Fischer). One microgram of RNA was reverse-transcribed using an anchored 3′ RACE oligo(dT) primer. This was followed by two rounds of nested PCR using RUS-3'-RACE as forward and 3'-outer primers and 3'-inner as reverse primer. The PCR product was gel-purified and sequenced.

Generation of the RUS knockdown vector.

ShRNAs were designed according to standard procedures (Yuan *et al*, 2004). In brief, 100 pmol RUS-sh-FW and 100 pmol RUS-sh-RV were annealed in 50 µl NEB2.1. The annealed fragment was cloned into pLKO.1-TRC-Puro vector, linearized with AgeI and EcoRI (Moffat *et al*, 2006) and amplified in Dh5α. For pLKO.1 vectors containing GFP as a selection marker, the puromycin resistance gene was replaced with the GFP gene via BamHI and KpnI restriction sites. Towards this end, the GFP cDNA was amplified from pLenti-CMV-GFP-Hygro (Campeau *et al*, 2009) by PCR using the primers: BamH-GFP-fw and Kpn-GFP-rv.

Construction of pcDNA-5FRT-5xMS2.

pcDNA.5-FRT vectors used to generate stable FlpIN Neuro2 A cells were equipped with 5xMS2 stem-loops. The 3xMS2 stem-loop sequence was PCR-amplified with the primers MS2_fw and MS2_rv from pAdMl3-$(MS2)_3$, digested with BamHI and XbaI, and ligated to BamHI/XbaI-linearized pcDNA5-FRT. Upon amplification in Dh5α, one clone fortuitously expanded 3xMS2 stem-loops to 5xMS2 stem-loops. This clone was used.

Generation of RUS overexpression vector.

RUS and ∆5'*RUS* sequences were isolated from a hippocampal cDNA library by PCR with the primers: RUS-LIC-fw or ∆5' RUS-LIC-fw, respectively and RUS-LIC-rv and cloned into pcDNA-5-FRT or pcDNA.5-FRT-5xMS2 (Thermo Fischer) via LIC cloning (Wang *et al*, 2012) and amplified in Dh5α. The *RUS* cDNA was the shuffled into pLenti-CMV-GFP-Hygro (Campeau *et al*, 2009) via ClaI and ApaI restriction sites to replace GFP and the hygromycin resistance gene. All constructs were verified by sequencing.

Construction of pLenti-FRT.

pLenti-GFP-Puro (Campeau *et al*, 2009) was digested with XbaI and BamHI to remove GFP downstream of the CMV promoter. FRT site was generated by annealing the oligonucleotides FRT_fw and FRT_rv. For annealing, 100 pmol of each oligonucleotide was heated in 50 µl NEB 2.1 to 95°C for 5min and slowly cooled down. 2 µl annealing scale was ligated into 20 ng digested vector and transformed in Dh5α.

Production of lentiviral particles.

All lentiviral experiments were conducted according to standard protocols (Moffat *et al*, 2006) and approved by the Bavarian state. $3x10^6$ HEK293T cells were seeded in 8 ml DMEM-GlutMax supplemented with 8% FCS on a 10 cm culture dish. Per virus production, 4 10 cm dishes were seeded. Next day, 53 µg DNA in a molar ratio of 2:1:1 of lentiviral-vector:psPAX2:pMD2.G transfected into 50-70% confluent cells. The medium was changed next day. Two days after transfection, viral particles were purified by sedimentation (87.000 g, 2h) from the medium and dissolved in 200 µl TBS5 (50 mM Tris-HCl pH 7.8, 130 mM NaCl, 10 mM KCl, 5 mM $MgCl_2$, 10% BSA).

Subcellular fractionation.

Subcellular fractionation was adapted from (Gagnon *et al*, 2014). Briefly, cells were lysed in ice-cold hypotonic lysis buffer (HLB; 10 mM Tris-HCl pH 7.5, 10 mM NaCl, 3 mM $MgCl_2$, 0.3% NP-40, 10% glycerol) for 10 min on ice. The cytoplasm was harvested by centrifugation (1000 g, 5 min) and the nuclear pellet was washed thrice in HLB. Nuclei were incubated in ice-cold Modified Wuarin-Schibler buffer (MWS; 10 mM Tris-HCl pH 7.5, 4 mM EDTA, 0.3 M NaCl, 1 M urea, 1% NP-40) for 15 min on ice. The nucleoplasm was separated from the chromatin by centrifugation (1000 g, 5 min). The RNA in the cytoplasmic and nucleoplasmic fractions was ethanol-precipitated and subjected along with the chromatin pellet for RNA purification.

RNA-seq analysis.

Total RNA was isolated and polyA-enriched. After reverse transcription, the cDNA was fragmented, end-repaired, and polyA-tailed. Solexa sequencing adaptors were ligated, and adaptor-modified fragments were enriched by 10-18 cycles of PCR amplification. Quantity and the size of the sequencing library were accessed on a Bioanalyzer before sequencing on an Illumina NextSeq 500 platform. Sequencing reads from FASTAQ files were aligned the STAR Aligner version (Dobin *et al*, 2013) and quantified using rsem (Li & Dewey, 2011). The reference genome used for alignment was constructed using the mm10 fasta file and GRCm38.99 transcript table. Quantified values were further statistically evaluated using Bioconductor's DeSeq2 package (Love *et al*, 2014). Expression changes with an FDR < 0.05 were considered significant. Among them, genes with a stat < -2 or >2 were extracted as down- or upregulated genes, respectively (Table EV2).

Gene ontology term enrichment analysis.

GO enrichment employed the web-based PANTHER software (Mi *et al*, 2013). The deregulated genes enriching for GO terms of interest were extracted from the provided xml file and matched to their expression values using R.

ChIRP-seq analysis.

NSCs from 8 x 15 cm dishes were harvested 7 days after seeding and washed twice with PBS. Cells were crosslinked in 100 ml 1% glutaraldehyde for 10 min at RT. Crosslinking was quenched 125 mM glycine for 5 min. Cells were pelleted at 1000 g for 5 min. ChIRP was done according to (Chu *et al*, 2011). Crosslinked cells were washed twice in PBS and lysed in 2 ml ChIRP-lysis buffer (50 mM Tris-HCl pH 7.0, 10 mM EDTA, 1% SDS, 1 mM PMSF, 1x protease inhibitor, SuperaseIn 100 U/ml). Chromatin shearing by Bioruptor typically yielded fragments of 150-600 bp. Sheared chromatin was diluted with 4 ml ChIRP-hybridization buffer (50 mM Tris-HCl pH 7.0, 750 mM NaCl, 15% (m/v) formamide, 1 mM EDTA, 1% SDS, with protease and RNase inhibitors) and divided into two aliquots, which were hybridized with 100 pmol biotinylated 'odd' and 'even' probe sets, respectively, at 37°C for 4 h with continuous rotation. Then 1 mg of magnetic streptavidin bead suspension (Thermo Fischer) in ChIRP-Lysis buffer were added and incubated for 30 min at 37°C with continuous rotation. Beads were washed 5 times with 1 ml ChIRP Wash buffer (300 mM NaCl, 30 mM Na_3-citrate, 0.1% SDS, 1 mM PMSF) for 5 min at 37°C. 90% of bead material was used for DNA isolation and 10% for RNA isolation. The enrichment of *RUS*, TBP mRNA, *MALAT*, and *XIST* was analyzed by RT-qPCR.

Isolated DNA was processed alongside an input chromatin sample. Ends were blunted with T4 DNA polymerase and polynucleotide kinase and an AMP was added. Solexa sequencing adaptors were ligated and adaptor-modified fragments were enriched by 10-18 cycles of PCR amplification. Sequencing libraries were size-selected on AMPure Beads (Beckman Coulter), quality-controlled on a Bioanalyzer (Agilent) and sequenced on an Illumina NextSeq-500 platform.

Sequencing reads from FASTQ files were aligned with bowtie2 (Langmead & Salzberg, 2012) to mm10. Multimapping reads were removed using samtools (Li *et al*, 2009). ChIRP peaks were called with MACS1.4 for both probe sets independently (Feng *et al*, 2012). The deeptools package was used to generate the bedgaph files (Ramírez *et al*, 2016). Bedtools (Quinlan & Hall, 2010) and python 2.7 matched even and odd bedgraph files into a single bedgraph file via the 'take-lower' method. The experiment was done in triplicates Only peaks occurring in each even and odd sample and in all three data sets called with Bioconductor's

GenomicRanges package (Lawrence *et al*, 2013) were considered valid *RUS* binding sites. The overlap demanded a minimal distance of 200 bp between the 'even' and 'odd' summit. Probe sequences within overlapping peaks were detected using Fimo (Grant *et al*, 2011) of the MEME software (Bailey *et al*, 2015) and removed using a cutoff of p <1e-8 before further analysis using GenomicRanges (Lawrence *et al*, 2013).

Filtered peaks were annotated with Homer (Heinz *et al*, 2010) using mm10 as reference genome (Table EV3). The obtained annotation statistic was used to calculate the distribution of *RUS* peaks within promoter, intergenic, intron, and close to repetitive sites. The annotated neighboring genes of *RUS* peaks were considered putative *RUS* target genes. GO term enrichment of putative target genes employed the web-based PANTHER software (Mi et al, 2013). Next, putative target gene expression and changes upon in shRNA^{CON} and shRNA^{RUS} treatment on day 5 and 7 were extracted from the RNA-seq data using the R-package SummarizedExperiments and DeSeq2 (Table EV3). Expression changes with an FDR < 0.05 were considered significant. Among them, genes with a stat < -2 or >2 were considered as down- or upregulated genes. Expression values of both time points were merged, log2-transformed and ranked by hierarchically clustering using the Euclidean Distance method in R. Furthermore, the correlation between *RUS* and putative target gene expression was calculated using the Pearson correlation coefficient on both time points separately (Table EV3).

MS2 Affinity purification of RUS interactors.

Stable pools of Neuro2A cells expressing 5xMS2-tagged *RUS* were generated as follows. 5x10^4 Neuro2A cells were transfected with 5 µl pLenti-FRT virus and 2 days later selected in GlutMax, 8% FCS supplemented with 2 µg/ml puromycin and expanded. 10^6 Neuro2A-FRT cells were seeded on a 10 cm culture dish. On the next day, cells were transfected with 15 µg plasmid DNA, consisting of a molar ratio of 1:6 (up to 1:9) of pcDNA5-lncRNA-5xMS2: pCSFLPe (encoding the flipase). Plasmids were diluted appropriately in 300 µl 150 mM NaCl and 15 µl JetPEI (2.6 µg/µl) and mixed. After 30 min equilibration at RT, the solution was added dropwise to Neuro2-FRT cells. Two days later, cells were transferred to a new 10 cm dish and selected in GlutMax 8% FCS, 2 µg/ml puromycin, and 600 µg/ml hygromycin. The medium was replaced every second day to remove cell debris. Colonies formed 7-10 days after transfection. They were harvested and further cultivated.

Nuclear extract from MS2-tagged *RUS*-expressing Neuro2A cells was prepared typically from 8x10^7 cells without dialysis, according to (Dignam *et al*, 1983). Extract preparation and MS2-affinity purification were done at 4°C. Cell pellets were suspended in 5 vol buffer A (10 mM HEPES pH 7.9 at 4°C, 1.5 mM $MgCl_2$, 10 mM KCl, 0.5 mM DTT, 200 U/ml RNAsin) and incubated for 10 min. Cells were homogenized with a Dounce tissue grinder. Nuclei were pelleted at 500 g for 10 min, washed with 5 nuclear volumes (vol) buffer A, dissolved in one vol buffer C (20 mM HEPES pH 7.9, 25% (v/v) glycerol, 0.42 M KCl, 1.5 mM $MgCl_2$, 0.2 mM EDTA, 0.5 mM PMSF, 0.5 mM DTT, 200 U/ml RNAsin) and homogenized again with a Dounce tissue grinder. After gentle rotation for 30 min, chromatin was pelleted at 17.000 g for 30 min. The supernatant was diluted with 1 vol buffer G (20 mM HEPES pH 7.9, 20% (v/v) glycerol, 0.2 mM EDTA, 0.5 mM PMSF, 0.5 mM DTT, 200 U/ml RNAsin) and used for affinity purification.

Standard MS2-affinity purification was done on supernatant containing 1 mg protein. To this, 760 pmol yeast t-RNA competitor and 120 pmol recombinant MS2BP-MBP (Jurica *et al*, 2002; Zhou & Reed, 2003) was added. After 2 h of gentle rotation, 50 µl equilibrated amylose resin (New England Biolabs) was added and incubation continued for 2 h. The resin was

pelleted at 1900 g for 1 min and washed thrice with 900 µl buffer D (buffer G containing 0.1 M KCl and lacking RNasin) and thrice 900 µl buffer F (buffer D containing 1.5 mM $MgCl_2$,).

RNA-interacting proteins were identified by mass spectrometry. Interacting proteins were eluted with 50 µg RNAse A in 80 µl buffer D at 37°C for 10 min. The resin was pelleted at 1900 g for 1 min at 4°C and the supernatant subjected to Filter Aided Sample Preparation (Wiśniewski *et al*, 2009) and peptides were desalted using C18 StageTips, dried by vacuum centrifugation and dissolved in 20 µL 0.1% formic acid. Samples were analyzed on a Easy nLC 1000 coupled online to a Q-Exactive mass spectrometer (Thermo Scientific, US). Eight µl peptide solution per sample were separated on a self-packed C18 column (30 cm × 75 µm; ReproSil-Pur 120 C18-AQ, 1.9 µm, Dr. Maisch GmbH, Germany) using a 180 min binary gradient of water and acetonitrile supplemented with 0.1% formic acid (0 min., 2% B; 3:30 min., 5% B; 137:30 min., 25% B; 168:30 min., 35% B; 182:30 min., 60% B) at 50 °C column temperature. A top 10 DDA method was used. Full scan MS spectra were acquired with a resolution of 70,000. Fragment ion spectra were recorded using a 2 m/z isolation window, 75 ms maximum trapping time with an AGC target of 10^5 ions.

The Raw Data were analyzed with the MaxQuant (version 2.0.1.0) software (Cox & Mann, 2008) using a one protein per gene canonical database of Mus musculus from Uniprot (download : 2021-04-09; 21998 entries). Trypsin was defined as protease. Two missed cleavages were allowed for the database search. The option first search was used to recalibrate the peptide masses within a window of 20 ppm. For the main search peptide and peptide fragment mass tolerances were set to 4.5 and 20 ppm, respectively. Carbamidomethylation of cysteine was defined as a static modification. Acetylation of the protein N-terminus as well as oxidation of methionine set as variable modifications. Match between runs was enabled with a retention time window of 1 min. Two ratio counts of unique peptides were required for label-free quantification (LFQ).

Output files were further analyzed using the software Perseus (Tyanova *et al*, 2016). Proteins identified by site, reverse matching peptides and contaminants were removed and LFQ intensities were log2 transformed. Next, only protein groups with 5 out of 5 quantifications in one condition were considered for relative protein quantification. To account for proteins that were only consistently quantified in one condition, data imputation was used with a down-shift of 2 and a width of 0.2. A permuation based FDR correction (Tusher *et al*, 2001) for multiple hypotheses was applied (p = 0.05; s0 = 0.1). Proteins were considered enriched if the fold change was greater than two and the p-value less than 0.002 (Table EV4).

RNA immunoprecipitation.

Protein A/G-Agarose beads (35 µl, Thermo Fischer) were blocked overnight with 1% BSA in buffer D. To nuclear extract from $5x10^6$ NSC 760 pmol yeast t-RNA, 300 µg salmon sperm DNA and 4 µg Lbr antibody was added and incubated for 2 h at 4°C under gentle rotation. Anti-rabbit IgG was used as a negative control. The binding reaction was added to blocked Protein A/G-Agarose and incubated for 2 h at 4°C with gentle rotation. Protein A/G beads were sedimented, washed 5x with 900 µl buffer D, suspended in 800 µl Trizol and subject to RNA extraction. RUS levels were analyzed by RT-PCR analysis and compared against the IgG purification. The experiment was performed in triplicates and statistically evaluated by a one-tailored student's t-test using Bonferroni p-value adjustment.

Acknowledgements

We thank Aline Campos, Silke Krause and Anna Berghofer for technical assistance, Tobias Straub for advice on bioinformatic analysis, Bianka Baying, Vladimir Benes (EMBL GeneCore), and Stefan Krebs (LAFUGA) for library preparation and sequencing and Christian Haass for his continued support. We are grateful to Sandra Schick, Marie Kube and Rodrigo Villaseñor for critical reading of the manuscript. This work was funded by the Deutsche Forschungsgemeinschaft (DFG) within the framework of the Munich Cluster for Systems Neurology (EXC 2145 SyNergy– ID 390857198), grant Be1140/8-1 (to PBB) and the Adele Hartmann Programm of the LMU (to JCS).

Author contributions

JCS and MS conceived the study. MS and VM performed experiments. MS analyzed and interpreted all experiments. SAM and SFL performed LC-MS analysis. MS and PBB wrote the manuscript. All authors proofread the manuscript.

Conflict of interest

The authors declare no conflict of interest.

Data Availability Section

The datasets and computer code produced in this study are available in the following databases:

- RNA-Seq data: Gene Expression Omnibus GSE196487 (https://www.ncbi.nlm.nih.gov/geo/query/acc.cgi?acc=GSE196487, reviewer access token : szajouyirxsjfqj)
- ChiRP-Seq data: Gene Expression Omnibus GSE196527 (https://www.ncbi.nlm.nih.gov/geo/query/acc.cgi?acc=GSE196527 , reviewer access token: kbytkaqghfgfzuf)
- Protein interaction AP-MS data: PRIDE PXD031664 (Perez-Riverol *et al*, 2022) (http://www.ebi.ac.uk/pride/archive/projects/PXD000208, reviewer access: username: reviewer_pxd031664@ebi.ac.uk, password: 6p26fYpI)
- Computer scripts: GitHub (https://github.com/MariusFSchneider/Schneider22)

References

Andrews BJ, Proteau GA, Beatty LG & Sadowski PD (1985) The FLP recombinase of the 2μ circle DNA of yeast: Interaction with its target sequences. *Cell* 40: 795–803

Antonelli F, Casciati A, Tanori M, Tanno B, Linares-Vidal M V, Serra N, Bellés M, Pannicelli A, Saran A & Pazzaglia S (2018) Alterations in Morphology and Adult Neurogenesis in the Dentate Gyrus of Patched1 Heterozygous Mice. *Front Mol Neurosci* 11: 168

Aruga J, Yokota N & Mikoshiba K (2003) Human SLITRK family genes: Genomic organization and expression profiling in normal brain and brain tumor tissue. *Gene* 315: 87–94

Azari H, Osborne GW, Yasuda T, Golmohammadi MG, Rahman M, Deleyrolle LP, Esfandiari E, Adams DJ, Scheffler B, Steindler DA, *et al* (2011) Purification of immature neuronal cells from neural stem cell progeny. *PLoS One* 6

Bailey TL, Johnson J, Grant CE & Noble WS (2015) The MEME Suite. *Nucleic Acids Res* 43: W39–W49

Briggs JA, Wolvetang EJ, Mattick JS, Rinn JL & Barry G (2015) Mechanisms of Long Non-coding RNAs in Mammalian Nervous System Development, Plasticity, Disease, and Evolution. *Neuron* 88: 861–877

Campeau E, Ruhl VE, Rodier F, Smith CL, Rahmberg BL, Fuss JO, Campisi J, Yaswen P, Cooper PK & Kaufman PD (2009) A Versatile Viral System for Expression and Depletion of Proteins in Mammalian Cells. *PLoS One* 4: e6529

Ceballos-Chávez M, Rivero S, García-Gutiérrez P, Rodríguez-Paredes M, García-Domínguez M, Bhattacharya S & Reyes JC (2012) Control of neuronal differentiation by sumoylation of BRAF35, a subunit of the LSD1-CoREST histone demethylase complex. *Proc Natl Acad Sci U S A* 109: 8085–8090

Chen J, Dong X, Cheng X, Zhu Q, Zhang J, Li Q, Huang X, Wang M, Li L, Guo W, *et al* (2021) Ogt controls neural stem/progenitor cell pool and adult neurogenesis through modulating Notch signaling. *Cell Rep* 34: 108905

Chou S-M, Li K-X, Huang M-Y, Chen C, King Y-HL, Li GG, Zhou W, Teo CF, Jan YN, Jan LY, *et al* (2021) Kv1.1 channels regulate early postnatal neurogenesis in mouse hippocampus via the (TrkB) signaling pathway. *Elife* 10: e58779

Chu C, Qu K, Zhong FL, Artandi SE & Chang HY (2011) Genomic maps of long noncoding RNA occupancy reveal principles of RNA-chromatin interactions. *Mol Cell* 44: 667–78

Chun-Kan C, Mario B, Constanza J, Erik A, Noah O, Christine S, Amy C, Andrea C, Patrick M & Mitchell G (2016) Xist recruits the X chromosome to the nuclear lamina to enable chromosome-wide silencing. *Science (80-)* 354: 468–472

Clark BS & Blackshaw S (2017) Understanding the Role of lncRNAs in Nervous System Development. In *Long Non Coding RNA Biology* pp 253–282. Singapour: Springer Nature Singapore Pte Ltd

Cox J & Mann M (2008) MaxQuant enables high peptide identification rates, individualized p.p.b.-range mass accuracies and proteome-wide protein quantification. *Nat Biotechnol* 26: 1367–1372

Cox J & Mann M (2009) Computational principles of determining and improving mass precision and accuracy for proteome measurements in an Orbitrap. *J Am Soc Mass Spectrom* 20: 1477–85

Dignam JD, Lebovitz RM & Roeder RG (1983) Accurate transcription initiation by RNA polymerase II in a soluble extract from isolated mammalian nuclei. *Nucleic Acids Res* 11: 1475–1489

Djebali S, Davis C a., Merkel A, Dobin A, Lassmann T, Mortazavi A, Tanzer A, Lagarde J, Lin W, Schlesinger F, *et al* (2012) Landscape of transcription in human cells. *Nature* 489: 101–108

Dobin A, Davis CA, Schlesinger F, Drenkow J, Zaleski C, Jha S, Batut P, Chaisson M & Gingeras TR (2013) STAR: Ultrafast universal RNA-seq aligner. *Bioinformatics* 29: 15–21

Engler A, Rolando C, Giachino C, Saotome I, Erni A, Brien C, Zhang R, Zimber-Strobl U, Radtke F, Artavanis-Tsakonas S, *et al* (2018) Notch2 Signaling Maintains NSC Quiescence in the Murine Ventricular-Subventricular Zone. *Cell Rep* 22: 992–1002

Engreitz JM, Ollikainen N & Guttman M (2016) Long non-coding RNAs: Spatial amplifiers that control nuclear structure and gene expression. *Nat Rev Mol Cell Biol* 17: 756–770

Eriksson PS, Perfilieva E, Björk-Eriksson T, Alborn A-M, Nordborg C, Peterson DA & Gage FH (1998) Neurogenesis in the adult human hippocampus. *Nat Med* 4: 1313–1317

Feng J, Liu T, Qin B, Zhang Y & Liu XS (2012) Identifying ChIP-seq enrichment using MACS. *Nat Protoc* 7: 1728–1740

Franks TM, McCloskey A, Shokirev M, Benner C, Rathore A & Hetzer MW (2017) Nup98 recruits the Wdr82-Set1A/COMPASS complex to promoters to regulate H3K4 trimethylation in hematopoietic progenitor cells. *Genes Dev* 31: 2222–2234

Fusaro G, Dasgupta P, Rastogi S, Joshi B & Chellappan S (2003) Prohibitin Induces the Transcriptional Activity of p53 and Is Exported from the Nucleus upon Apoptotic Signaling. *J Biol Chem* 278: 47853–47861

Gagnon KT, Li L, Janowski BA & Corey DR (2014) Analysis of nuclear RNA interference in human

cells by subcellular fractionation and Argonaute loading. *Nat Protoc* 9: 2045–2060

Galichet C, Guillemot F & Parras CM (2008) Neurogenin 2 has an essential role in development of the dentate gyrus. *Development* 135: 2031–2041

Garay PM, Wallner MA & Iwase S (2016) Yin–yang actions of histone methylation regulatory complexes in the brain. *Epigenomics* 8: 1689–1708

Gozalo A, Duke A, Lan Y, Pascual-Garcia P, Talamas JA, Nguyen SC, Shah PP, Jain R, Joyce EF & Capelson M (2020) Core Components of the Nuclear Pore Bind Distinct States of Chromatin and Contribute to Polycomb Repression. *Mol Cell* 77: 67-81.e7

Grant CE, Bailey TL & Noble WS (2011) FIMO: Scanning for occurrences of a given motif. *Bioinformatics* 27: 1017–1018

Hatakeyama J & Kageyama R (2006) Notch1 Expression Is Spatiotemporally Correlated with Neurogenesis and Negatively Regulated by Notch1-Independent Hes Genes in the Developing Nervous System. *Cereb Cortex* 16: i132--i137

Heinz S, Benner C, Spann N, Bertolino E, Lin YC, Laslo P, Cheng JX, Murre C, Singh H & Glass CK (2010) Simple Combinations of Lineage-Determining Transcription Factors Prime cis-Regulatory Elements Required for Macrophage and B Cell Identities. *Mol Cell* 38: 576–589

Hezroni H, Perry RBT & Ulitsky I (2019) Long noncoding RNAs in development and regeneration of the neural lineage. *Cold Spring Harb Symp Quant Biol* 84: 165–177

Hublitz P, Kunowska N, Mayer UP, Müller JM, Heyne K, Yin N, Fritzsche C, Poli C, Miguet L, Schupp IW, *et al* (2005) NIR is a novel INHAT repressor that modulates the transcriptional activity of p53. *Genes Dev* 19: 2912–2924

Imura T, Kornblum HI & Sofroniew M V. (2003) The predominant neural stem cell isolated from postnatal and adult forebrain but not early embryonic forebrain expresses GFAP. *J Neurosci* 23: 2824–2832

Ivanov D (2019) Notch Signaling-Induced Oscillatory Gene Expression May Drive Neurogenesis in the Developing Retina. *Front Mol Neurosci* 12: 226

Johansson HE, Liljas L & Uhlenbeck OC (1997) RNA recognition by the MS2 phage coat protein. *Semin Virol* 8: 176–185

Johe KK, Hazel TG, Muller T, Dugich-Djordjevic MM & McKay RDG (1996) Single factors direct the differentiation of stem cells from the fetal and adult central nervous system. *Genes Dev* 10: 3129–3140

Jurica MS, Licklider LJ, Gygi SP, Grigorieff N & Moore MJ (2002) Purification and characterization of native spliceosomes suitable for three-dimensional structural analysis. *Rna* 8: 426–439

Kilpatrick TJ & Bartlett PF (1993) Cloning and growth of multipotential neural precursors: Requirements for proliferation and differentiation. *Neuron* 10: 255–265

Kind J, Pagie L, Ortabozkoyun H, Boyle S, De Vries SS, Janssen H, Amendola M, Nolen LD, Bickmore WA & Van Steensel B (2013) Single-cell dynamics of genome-nuclear lamina interactions. *Cell* 153: 178–192

Kopp F & Mendell JT (2018) Functional Classification and Experimental Dissection of Long Noncoding RNAs. *Cell* 172: 393–407

Koushyar S, Jiang WG & Dart DA (2015) Unveiling the potential of prohibitin in cancer. *Cancer Lett* 369: 316–322

Langmead B & Salzberg SL (2012) Fast gapped-read alignment with Bowtie 2. *Nat Methods* 9: 357–359

Lawrence M, Huber W, Pagès H, Aboyoun P, Carlson M, Gentleman R, Morgan MT & Carey VJ (2013) Software for Computing and Annotating Genomic Ranges. *PLoS Comput Biol* 9: 1–10

Li B & Dewey CN (2011) RSEM: accurate transcript quantification from RNA-Seq data with or without a reference genome. *BMC Bioinformatics* 12: 323

Li H, Handsaker B, Wysoker A, Fennell T, Ruan J, Homer N, Marth G, Abecasis G & Durbin R (2009) The Sequence Alignment/Map format and SAMtools. *Bioinformatics* 25: 2078–2079

Lin N, Chang KY, Li Z, Gates K, Rana Z, Dang J, Zhang D, Han T, Yang CS, Cunningham TJ, *et al* (2014) An evolutionarily conserved long noncoding RNA TUNA controls pluripotency and neural lineage commitment. *Mol Cell* 53: 1005–1019

Liu Z, Yan M, Liang Y, Liu M, Zhang K, Shao D, Jiang R, Li L, Wang C, Nussenzveig DR, *et al* (2019) Nucleoporin Seh1 Interacts with Olig2/Brd7 to Promote Oligodendrocyte Differentiation and Myelination. *Neuron* 102: 587-601.e7

Love MI, Huber W & Anders S (2014) Moderated estimation of fold change and dispersion for RNA-seq data with DESeq2. *Genome Biol* 15: 1–21

MacArthur IC, Bei Y, Garcia HD, Ortiz M V., Toedling J, Klironomos F, Rolff J, Eggert A, Schulte JH, Kentsis A, *et al* (2019) Prohibitin promotes dedifferentiation and is a potential therapeutic target in neuroblastoma. *JCI Insight* 4: e127130

Mamber C, Kamphuis W, Haring NL, Peprah N, Middeldorp J & Hol EM (2012) GFAPδ Expression in Glia of the Developmental and Adolescent Mouse Brain. *PLoS One* 7: 1–15

Markaki Y, Gan Chong J, Wang Y, Jacobson EC, Luong C, Tan SYX, Jachowicz JW, Strehle M, Maestrini D, Banerjee AK, *et al* (2021) Xist nucleates local protein gradients to propagate silencing across the X chromosome. *Cell* 184: 6174-6192.e32

Mase S, Shitamukai A, Wu Q, Morimoto M, Gridley T & Matsuzaki F (2021) Notch1 and Notch2 collaboratively maintain radial glial cells in mouse neurogenesis. *Neurosci Res* 170: 122–132

Mercer TR, Qureshi I a, Gokhan S, Dinger ME, Li G, Mattick JS & Mehler MF (2010) Long noncoding RNAs in neuronal-glial fate specification and oligodendrocyte lineage maturation. *BMC Neurosci* 11: 14

Mi H, Muruganujan A & Thomas PD (2013) PANTHER in 2013: Modeling the evolution of gene function, and other gene attributes, in the context of phylogenetic trees. *Nucleic Acids Res* 41: 377–386

Moffat J, Grueneberg D a., Yang X, Kim SY, Kloepfer AM, Hinkle G, Piqani B, Eisenhaure TM, Luo B, Grenier JK, *et al* (2006) A Lentiviral RNAi Library for Human and Mouse Genes Applied to an Arrayed Viral High-Content Screen. *Cell* 124: 1283–1298

Mukherjee S, Brulet R, Zhang L & Hsieh J (2016) REST regulation of gene networks in adult neural stem cells. *Nat Commun* 7: 1–14

Mukhtar T, Breda J, Grison A, Karimaddini Z, Grobecker P, Iber D, Beisel C, van Nimwegen E & Taylor V (2020) Tead transcription factors differentially regulate cortical development. *Sci Rep* 10: 1–19

Ng SY, Bogu GK, Soh BS & Stanton LW (2013) The long noncoding RNA RMST interacts with SOX2 to regulate neurogenesis. *Mol Cell* 51: 349–359

Palazzo AF & Koonin E V. (2020) Functional Long Non-coding RNAs Evolve from Junk Transcripts. *Cell* 183: 1151–1161

Pascual-Garcia P & Capelson M (2021) The nuclear pore complex and the genome: organizing and regulatory principles. *Curr Opin Genet Dev* 67: 142–150

Pascual-Garcia P, Debo B, Aleman JR, Talamas JA, Lan Y, Nguyen NH, Won KJ & Capelson M (2017) Metazoan Nuclear Pores Provide a Scaffold for Poised Genes and Mediate Induced Enhancer-Promoter Contacts. *Mol Cell* 66: 63-76.e6

Perez-Riverol Y, Bai J, Bandla C, García-Seisdedos D, Hewapathirana S, Kamatchinathan S, Kundu DJ, Prakash A, Frericks-Zipper A, Eisenacher M, *et al* (2022) The PRIDE database resources in 2022: a hub for mass spectrometry-based proteomics evidences. *Nucleic Acids Res* 50: D543–D552

Ponjavic J, Oliver PL, Lunter G & Ponting CP (2009) Genomic and Transcriptional Co-Localization of Protein-Coding and Long Non-Coding RNA Pairs in the Developing Brain. *PLOS Genet* 5: e1000617

Price RL, Bhan A & Mandal SS (2021) HOTAIR beyond repression: In protein degradation, inflammation, DNA damage response, and cell signaling. *DNA Repair (Amst)* 105: 103141

Quinlan AR & Hall IM (2010) BEDTools: A flexible suite of utilities for comparing genomic features. *Bioinformatics* 26: 841–842

Quinn JJ & Chang HY (2016) Unique features of long non-coding RNA biogenesis and function. *Nat Rev Genet* 17: 47–62

Raducu M, Fung E, Serres S, Infante P, Barberis A, Fischer R, Bristow C, Thézénas M, Finta C, Christianson JC, *et al* (2016) SCF (Fbxl17) ubiquitylation of Sufu regulates Hedgehog signaling and medulloblastoma development . *EMBO J* 35: 1400–1416

Rajalingam K & Rudel T (2005) Ras-Raf signaling needs prohibitin. *Cell Cycle* 4: 1503–1505

Ramírez F, Ryan DP, Grüning B, Bhardwaj V, Kilpert F, Richter AS, Heyne S, Dündar F & Manke T (2016) deepTools2: a next generation web server for deep-sequencing data analysis. *Nucleic Acids Res* 44: W160–W165

Ramos AD, Andersen RE, Liu SJ, Nowakowski TJ, Hong SJ, Gertz CC, Salinas RD, Zarabi H, Kriegstein AR & Lim DA (2015) The long noncoding RNA Pnky regulates neuronal differentiation of embryonic and postnatal neural stem cells. *Cell Stem Cell* 16: 439–447

Rani N, Nowakowski TJ, Zhou H, Godshalk SE, Lisi V, Kriegstein AR & Kosik KS (2016) A Primate lncRNA Mediates Notch Signaling during Neuronal Development by Sequestering miRNA. *Neuron* 90: 1174–1188

Rinn JL & Chang HY (2012) Genome regulation by long noncoding RNAs. *Annu Rev Biochem* 81: 145–166

Rinn JL & Chang HY (2020) Long Noncoding RNAs: Molecular Modalities to Organismal Functions. *Annu Rev Biochem* 89: 283–308

Rutenberg-Schoenberg M, Sexton AN & Simon MD (2016) The Properties of Long Noncoding RNAs That Regulate Chromatin. *Annu Rev Genomics Hum Genet* 17: 69–94

Sauer B (1994) Site-specific recombination: developments and applications. *Curr Opin Biotechnol* 5: 521–527

Schoenherr CJ & Anderson DJ (1995) The neuron-restrictive silencer factor (NRSF): a coordinate repressor of multiple neuron-specific genes. *Science* 267: 1360–1363

See RH, Caday-Malcolm RA, Singaraja RR, Zhou S, Silverston A, Huber MT, Moran J, James ER, Janoo R, Savill JM, *et al* (2002) Protein kinase A site-specific phosphorylation regulates ATP-binding cassette A1 (ABCA1)-mediated phospholipid efflux. *J Biol Chem* 277: 41835–41842

Shin E, Kashiwagi Y, Kuriu T, Iwasaki H, Tanaka T, Koizumi H, Gleeson JG & Okabe S (2013) Doublecortin-like kinase enhances dendritic remodelling and negatively regulates synapse maturation. *Nat Commun* 4: 1440

Statello L, Guo CJ, Chen LL & Huarte M (2021) Gene regulation by long non-coding RNAs and its biological functions. *Nat Rev Mol Cell Biol* 22: 96–118

van Steensel B & Belmont AS (2017) Lamina-Associated Domains: Links with Chromosome Architecture, Heterochromatin, and Gene Repression. *Cell* 169: 780–791

Sueda R & Kageyama R (2019) Regulation of active and quiescent somatic stem cells by Notch signaling. *Dev Growth Differ* 62: 59–66

Takagi M, Sueishi M, Saiwaki T, Kametaka A & Yoneda Y (2001) A Novel Nucleolar Protein, NIFK, Interacts with the Forkhead Associated Domain of Ki-67 Antigen in Mitosis. *J Biol Chem* 276: 25386–25391

Tsai BP, Wang X, Huang L & Waterman ML (2011) Quantitative profiling of in vivo-assembled RNA-protein complexes using a novel integrated proteomic approach. *Mol Cell Proteomics* 10: M110.007385

Tusher VG, Tibshirani R & Chu G (2001) Significance analysis of microarrays applied to the ionizing radiation response. *Proc Natl Acad Sci U S A* 98: 5116–5121

Tyanova S, Temu T, Sinitcyn P, Carlson A, Hein MY, Geiger T, Mann M & Cox J (2016) The Perseus computational platform for comprehensive analysis of (prote)omics data. *Nat Methods* 13: 731–40

Vertii A, Ou J, Yu J, Yan A, Pagès H, Liu H, Zhu LJ & Kaufman PD (2019) Two contrasting classes of nucleolus-associated domains in mouse fibroblast heterochromatin. *Genome Res* 29: 1235–1249

Wang J, He X, Luo Y & Yarbrough WG (2006) A novel ARF-binding protein (LZAP) alters ARF regulation of HDM2. *Biochem J* 393: 489–501

Wang L, Hou S & Han Y-G (2016) Hedgehog signaling promotes basal progenitor expansion and the growth and folding of the neocortex. *Nat Neurosci* 19: 888–896

Wang S, Fusaro G, Padmanabhan J & Chellappan SP (2002) Prohibitin co-localizes with Rb in the nucleus and recruits N-CoR and HDAC1 for transcriptional repression. *Oncogene* 21: 8388–8396

Wang T, Ma X, Zhu H, Li A, Du G & Chen J (2012) Available methods for assembling expression cassettes for synthetic biology. *Appl Microbiol Biotechnol* 93: 1853–1863

Werner MS & Ruthenburg AJ (2015) Nuclear Fractionation Reveals Thousands of Chromatin-Tethered Noncoding RNAs Adjacent to Active Genes. *Cell Rep* 12: 1089–1098

Wiśniewski JR, Zougman A, Nagaraj N & Mann M (2009) Universal sample preparation method for proteome analysis. *Nat Methods* 6: 359–362

Xi J, Xu Y, Guo Z, Li J, Wu Y, Sun Q, Wang Y, Chen M, Zhu S, Bian S, *et al* (2022) LncRNA SOX1-OT V1 acts as a decoy of HDAC10 to promote SOX1-dependent hESC neuronal differentiation . *EMBO Rep* 23: 1–17

Yao PJ, Petralia RS & Mattson MP (2016) Sonic Hedgehog Signaling and Hippocampal Neuroplasticity. *Trends Neurosci* 39: 840–850

Yao RW, Wang Y & Chen LL (2019) Cellular functions of long noncoding RNAs. *Nat Cell Biol* 21: 542–551

Yuan B, Latek R, Hossbach M, Tuschl T & Lewitter F (2004) siRNA selection server: An automated siRNA oligonucleotide predicition server. *Nucleic Acids Res* 32: 130–134

Zhou Z, Licklider LJ, Gygi SP & Reed R (2002) Comprehensive proteomic analysis of the human spliceosome. *Nature* 419: 182–185

Zhou Z & Reed R (2003) Purification of Functional RNA-Protein Complexes using MS2-MBP. *Curr Protoc Mol Biol* 63: 27.3.1-27.3.7

Ziller MJ, Edri R, Yaffe Y, Donaghey J, Pop R, Mallard W, Issner R, Gifford CA, Goren A, Xing J, *et al* (2015) Dissecting neural differentiation regulatory networks through epigenetic footprinting. *Nature* 518: 355–359

Zimmer-Bensch G (2019) Emerging Roles of Long Non-Coding RNAs as Drivers of Brain Evolution. *Cells* 8

Figure legends

Figure 1. RUS is a novel, conserved lncRNA involved in neurogenesis.

A. Workflow illustrating the criteria and selection principle applied to candidate lncRNAs (Ziller et al., 2015), which led to the selection of *RUS* as subject of this study.

B. Heatmap of significantly changed lncRNAs expressed in human ESC-derived NE, ERG, MRG and LRG before and after differentiation (two-sided t-test). Data of (Ziller et. al. 2015) were analysed.

C. Conservation of the *RUS* gene between mouse and human genomes by synteny (top) and by sequence of exon 1 (bottom). Note that the RUS gene resides just upstream of the *Slitrk3* gene in either case. For mice two *RUS* isoforms are indicated.

D. Expression of murine *RUS-1* and *RUS-2* isoforms (see panel C) in different embryonic (E-) and adult (A-) tissues: cortex (Cor), cerebellum (Cer), hippocampus (Hip), gut, heart, kidney, liver, lung, muscle, skin, spleen, analyzed by quantitative RT-PCR. The values were normalized to expression constitutive TBP mRNA (arbitrary units).

Figure 2. *RUS* is involved in neuronal development

A. Quantitative RT-PCR analysis of expression of *RUS*, *Map2*, *Gfap* and *Nestin* transcripts as indicated, during a 9-day time course of embryonic cortical NSC differentiation. Values were normalized to the maximal expression of each RNA during the time course. Error bars show the standard error of the mean of 3 independent experiments. FGF: Fibroblast growth factor.

B. Experimental strategy to deplete *RUS* in differentiating NSC by expressing shRNAs upon lentiviral transduction.

C. *RUS* levels determined by RT-qPCR in *RUS* knockdown cells (red, expressing shRNA^{RUS}) compared to control cells (blue, expressing a scrambled shRNA^{CON}). Error bars show the standard deviation of the mean of four individual experiments.

D. Left: Immunofluorescence visualization of β-tubulin III (upper panel) and Map2 (lower panel) in control (shRNA^{CON}) and knockdown (shRNA^{RUS}) cells using specific antibodies (magenta). Nuclei were stained with DAPI (4′,6-diamidin-2-phenylindol, blue). Scale bar = 25 µm.

Right: Quantification of percentage of immune-positive cells by ImageJ. The bar diagrams show the percentage of positive cells. Error bars show the standard deviation of four independent experiments.

E. Experimental strategy to rescue the *RUS*-depletion phenotype in differentiating NSC by lentiviral overexpression of *RUS*.

F. *RUS* levels were determined by RT-qPCR in control (shRNA^{CON}) and knockdown (shRNA^{RUS}) cells. Where indicated (+), *RUS* was overexpressed from a CMV promoter. Error bars show the standard deviation of four independent experiments. The dashed line highlights the level of *RUS* in (shRNA^{RUS}) cells

G. β-tubulin III immunostaining in control (shRNA^{CON}) and knockdown (shRNA^{RUS}) cells as a function of *RUS* overexpression. Nuclei are stained with DAPI. Scalebar = 50 µm)

H. Quantification of β-tubulin-III immunostaining of cultures as in G. Error bars show the standard deviation of four independent experiments (* $p < 0.05$, ** $p < 0.01$, *** $p < 0.005$).

Figure 3. Transcriptome changes upon depletion of *RUS*

A. Enriched gene ontology (GO) classifications among genes down-regulated (blue) or up-regulated (orange) upon *RUS* depletion at days 5 and day 7 of culture, as indicated. Circle size indicates the number of deregulated genes compared to the total number of genes enriched in the respective GO annotation (100% =1).

B. Heatmap showing the top 50 deregulated genes enriching for the GO annotations 'cell-death', 'neurogenesis', 'cell-cycle' and 'microtubule-based process' on day five (left) and day 7 (right) of culture. Note that these are different genes. The genes were sorted by GO annotations and difference between $shRNA^{CON}$and $shRNA^{RUS}$,.

C. Expression levels of the indicated marker genes on day 5 and day 7 of culture in control ($shRNA^{CON}$, blue) and knockdown ($shRNA^{RUS}$, red) cells were determined by RNA-seq (TPM values were normalized to those of the control cells on day 5. Error bars show the standard deviation)

Figure 4: Localization of *RUS* to chromosomal sites

A. Subcellular localization of *RUS*. NSCs were differentiated for two days and then fractionated into the sub-cellular compartments cytoplasm, nucleoplasm and chromatin. *RUS* was detected by RT-qPCR along with *Gapdh* mRNA (cytoplasmic marker) and *MALAT* (nuclear marker). Error bars: standard deviation of 3 independent experiments.

B. Genome annotation of the 94 high-confidence *RUS* ChIRP locations. SINE: short interspersed nuclear element; LINE: long interspersed nuclear element; LTR: long terminal repeat.

C. Browser view of two examples of *RUS* localization close to relevant neurogenic genes. The *RUS* ChIRP tag density of the three replicates is plotted I separate tracks in the genomic regions of the *Kcna1* (top) and *Dclk2* (bottom) genes. For orientation, the respective chromosomal regions are displayed above and the gene models below the traces.

D. Heatmap showing the expression changes of 66 *RUS* putative target genes upon *RUS* depletion ($shRNA^{RUS}$, red) or in control cells ($shRNA^{CON}$, blue) on days 5 and 7. Replicate identifiers are indicated below the columns. Genes were hierarchically clustered using Euclidean distance based on their combined expression on both days. This yields two clusters depending on whether genes are activated or repressed upon *RUS* depletion. The gene names are indicated to the right of the 7-day heatmap. The purple-green code to the right of each individual heatmap indicates the degree of correlation between *RUS* and putative target gene expression.

Figure 5: RUS interacts with components of the nuclear pore, -lamina, and nucleolus.

A. Schematic overview of the affinity purification of *RUS*-interacting proteins (colored spheres). *RUS* RNA (green), tagged with 5 MS2 stem-loop structures (orange) is stably expressed in Neuro2A cells. The RNA is affinity-purified by binding to MS2BP-maltose binding protein on an amylose resin. For details, see text.

B. Volcano plot showing affinity-purified nuclear proteins that bind differentially to full-length *RUS* (left) or a *RUS* RNA from which exon 1 was deleted *(Δ5'-RUS*). Proteins with a change greater than 2 and a p-value smaller than 0.002 are considered robust interactors and annotated by their gene name. The dashed gray hyperbolic curves depict a permutation-based false discovery rate estimation (P = 0.05; s0 = 1). Some proteins are color-coded: proteins of the nuclear lamina (red), nuclear porins (orange) and nucleolar proteins (green).

C. Quantitative RT-PCR analysis of *RUS* co-immunoprecipitated with antibodies against Sox2, Brd2, Lbr and control IgG from differentiating NSCs. Error bars show the standard deviation (*** p < 0.01 compared to IgG purification).

Tables and their legends

Table 1: Table includes affinity-purified nuclear proteins that bind more than full length *RUS* (p-value < 0.002, log2(mut/fl RUS) < -1) and the localization to nuclear compartments as nucleolus, nuclear lamin and nuclear pore. Table highlights whether a protein was identified by full-length *RUS* only.

Table 2: Reagents and Tools table

Table EV1: Used oligonucleotides

Table EV2: Differential gene expression analysis measured by RNASeq

Table EV3: RUS genomic binding sites measured by ChIRP-Seq and expression of putative target genes

Table EV4: Statistical evaluation of identified and quantified proteins after RUS affinity purifications by LC-MS.

Expanded View Figure legends

Figure EV1. Molecular characterization of RUS

A. Sequence of the *RUS* 3' end determined by 3' RACE.

B. Left: RT-PCR amplification of *RUS* using primers annealing to 5' and 3' ends, revealing the dominant isoform *RUS-1*. Right panel: Sequence of *RUS-1* (912 nt). Note that the annotated exon 4 is missing.

Figure EV2. Cell loss upon *RUS* depletion through reduced cell proliferation and increased apoptosis

A. Immunostaining of differentiating embryonic cortical NSC for the NSC marker nestin (magenta ,top row) ,the RGC marker Gfap (yellow, 2nd row), and for the neuronal markers Mapt (green, 3rd row) and β-tubulin III (red, bottom row) on the indicated days. Cell nuclei stained with 4′,6-Diamidin-2-phenylindol (DAPI), bar = 25 µm.

B. Quantitative RT-PCR analysis of mRNA encoding Dcx (double cortin), Gfap (glial fibrillary acidic protein), the glutamate transporter Glast, glutamate-ammonia ligase (GluL), Map2 (microtubule-associated protein 2), Mapt (microtubule-associated protein tau), nestin and β-tubulin III during differentiation of embryonic cortical NSC. Values are relative to the constitutively expressed TATA-binding protein (TBP) mRNA values in the same preparations, which were also used for normalization. Error bars: standard error of the mean of 3 independent experiments.

C. Experimental strategy to deplete *RUS* in differentiating NSC using lentiviral shRNAs. LTR: long terminal repeat, psi: packing signal, U6: U6-promoter, hPKG: human phosphoglycerate kinase promoter, Puro: puromycin resistance gene, GFP: Green fluorescent protein.

D. Quantification of BrdU immunostaining as a measure of replication. BrdU was added to differentiating NSC cultures on day 6 and its incorporation measured by immunostaining in control ($shRNA^{CON}$) and knockdown ($shRNA^{RUS}$) cells using specific antibodies (red). Nuclei were stained with DAPI. Scale bar = 25 µm. Images were quantified with ImageJ (right panel). Error bars show the standard deviation of three independent experiments (* $p < 0.05$, ** $p < 0.01$, *** $p < 0.005$).

E. Quantification of cleaved Caspase-3 immunostaining as a measure of apoptosis. Cleaved Caspase-3 was detected in GFP-expressing control ($shRNA^{CON}$) and knockdown ($shRNA^{RUS}$) cells using specific antibodies (magenta). Nuclei were stained with DAPI. Scale bar = 25 µm. The stainings were quantified with ImageJ (right panel). Error bars show the standard deviation of three independent experiments (* $p < 0.05$, ** $p < 0.01$, *** $p < 0.005$).

Figure EV3. Transcriptome changes upon depletion of RUS

A. Experimental strategy and timeline for transcriptome analysis.

B. *RUS* levels determined by RT-qPCR in *RUS* knockdown cells (red, expressing $shRNA^{RUS}$) compared to control cells (blue, expressing a scrambled $shRNA^{CON}$). Error bars show the standard deviation of the mean of four experiments.

C. Principle component analysis comparing RNA-seq profiles of cells treated with shRNA^{CON} (*CON*) or shRNA^{RUS} (*RUS*) on day 5 (left) or day 7 (right). The four replicates are labeled 1-4.

D. Heatmap displaying the relative expression of genes with significant deregulation (FDR < 0.05) on days five (left) and seven (right), hierarchically clustered using the Euclidean distance.

Figure EV4. Chromatin localization of RUS determined by ChIRP

A. Enrichment of *RUS*, *MALAT*, *TBP* mRNA, and *XIST* in ChIRP from differentiated NSC expressed as percent of the value obtained from input chromatin. Error bars: the standard deviation of 3 experiments.

B. Venn diagram showing the number of ChIRP peaks obtained in the three independent experiments and their overlap.

C. Browser view of two examples of *RUS* localization close to relevant neurogenic genes. The *RUS* ChIRP tag density of the three replicates is plotted in separate tracks in the genomic regions of the *Arid1b* (top) and *Bin1* (bottom) genes. For orientation, the respective chromosomal regions are displayed above and the gene models below the traces.

D. Correlation analyses showing the relationship between *RUS* expression and three selected putative target genes of cluster II, *App*, *Arid1* and *Kcna1,* in control (shRNA^{CON}) and *RUS* knockdown (shRNA^{RUS}) cells on day 5.

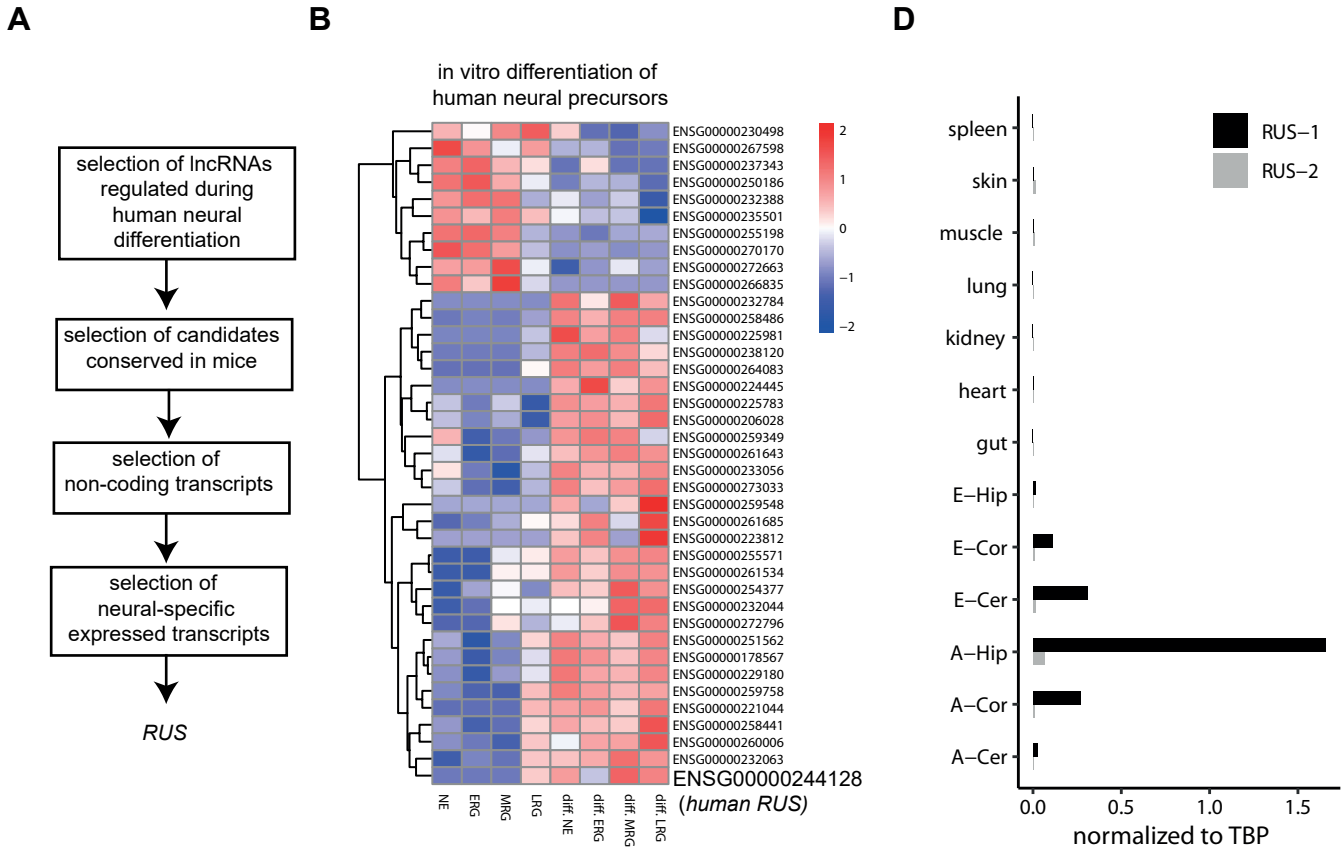
A
selection of lncRNAs regulated during human neural differentiation
selection of candidates conserved in mice
selection of non-coding transcripts
selection of neural-specific expressed transcripts
RUS
B
in vitro differentiation of human neural precursors
ENSG00000230498
ENSG00000267598
ENSG00000237343
ENSG00000250186
ENSG00000232388
ENSG00000235501
ENSG00000255198
ENSG00000270170
ENSG00000272663
ENSG00000266835
ENSG00000232784
ENSG00000258486
ENSG00000225981
ENSG00000238120
ENSG00000264083
ENSG00000224445
ENSG00000225783
ENSG00000206028
ENSG00000259349
ENSG00000261643
ENSG00000233056
ENSG00000273033
ENSG00000259548
ENSG00000261685
ENSG00000223812
ENSG00000255571
ENSG00000261534
ENSG00000254377
ENSG00000232044
ENSG00000272796
ENSG00000251562
ENSG00000178567
ENSG00000229180
ENSG00000259758
ENSG00000221044
ENSG00000258441
ENSG00000260006
ENSG00000232063
ENSG00000244128 (human RUS)
NE
ERG
MRG
LRG
diff.NE
diff.ERG
diff.MRG
diff.LRG
2
1
0
−1
−2
D
spleen
skin
muscle
lung
kidney
heart
gut
E−Hip
E−Cor
E−Cer
A−Hip
A−Cor
A−Cer
RUS−1
RUS−2
0.0
0.5
1.0
1.5
normalized to TBP
C
Mus musculus
Chr3:
73.00 Mb
73.10 Mb
73.20 Mb
73.30 Mb
73.40 Mb
73.50 Mb
73.60 Mb
73.70 Mb
Slitrk3
Gm20754 (RUS-1)
Gm20754 (RUS-2)
Bche-201
Homo sapiens
Chr3:
165.20 Mb
165.30 Mb
165.40 Mb
165.50 Mb
165.60 Mb
165.70 Mb
165.80 Mb
SLITRK3
LINC01322 (RUS)
Bche-201
mouse 10 GGGCTTAAGCCSGYTCRGCTCAGAGRTGGGTTTCGGRASTCTGTGGCGRASCASC-GCARCAAGTCATCACTCASYGTAYAAGYCTTTCCATTTCTGARARYAWAA--- 115
human 16 GGGCTTAATCCSGYGCRGCTCAGAGRTGGGTTTCTGRASTC----GCGRASCASCTGCARCAAGGCATCACTCASYGTAYAAGYATTTCCATTTCTGARARYAWAAGGA 121
mouse 116 AGAACTTAAGCRTGCGGCRYTYGGAGTGTARATTGCTTTGWRGTATTTCAARGCAGCRYTGATCATGGGCAGASGAGCTG 194
human 122 AGAACTTAAGCRGGCGGCRYTYGGAGTGTARATTGCTTTGWRGTATTTAAARGCAGARYGGATCCTGGGCAGCSGAGCTG 200
| exact match
: R (G-A), Y (C-T), S (G-C), W (A-T)

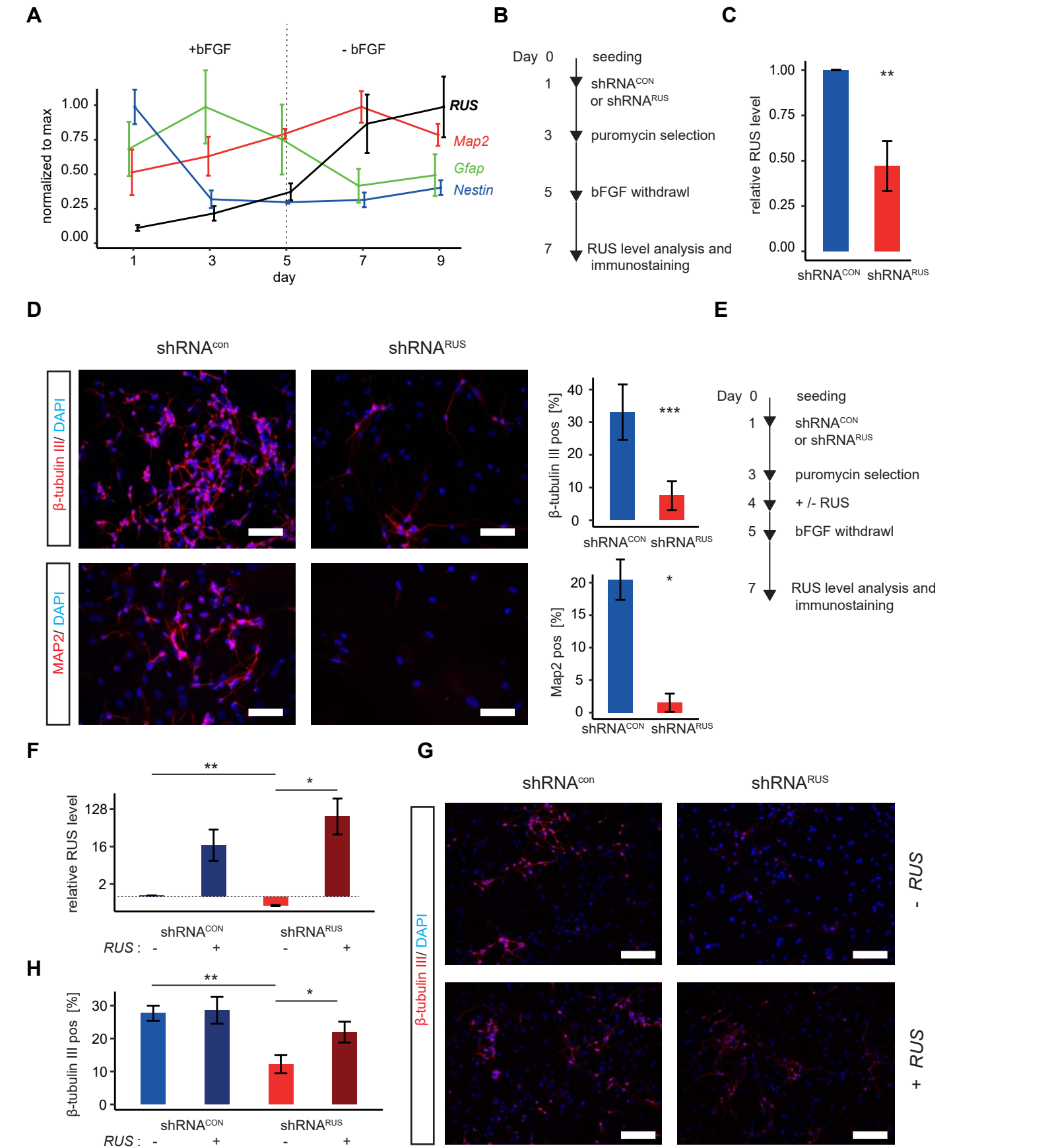
A
+bFGF
- bFGF
normalized to max
1.00
0.75
0.50
0.25
0.00
1
3
5
7
9
day
RUS
Map2
Gfap
Nestin
B
Day 0
seeding
1
shRNA^CON
or shRNA^RUS
3
puromycin selection
5
bFGF withdrawl
7
RUS level analysis and
immunostaining
C
relative RUS level
1.00
0.75
0.50
0.25
0.00
**
shRNA^CON
shRNA^RUS
D
shRNA^con
shRNA^RUS
β-tubulin III/ DAPI
MAP2/ DAPI
β-tubulin III pos [%]
40
30
20
10
0
***
shRNA^CON
shRNA^RUS
Map2 pos [%]
20
15
10
5
0
*
shRNA^CON
shRNA^RUS
E
Day 0
seeding
1
shRNA^CON
or shRNA^RUS
3
puromycin selection
4
+ /- RUS
5
bFGF withdrawl
7
RUS level analysis and
immunostaining
F
relative RUS level
128
16
2
**
*
shRNA^CON
shRNA^RUS
RUS : - + - +
G
shRNA^con
shRNA^RUS
β-tubulin III/ DAPI
- RUS
+ RUS
H
β-tubulin III pos [%]
30
20
10
0
**
*
shRNA^CON
shRNA^RUS
RUS : - + - +

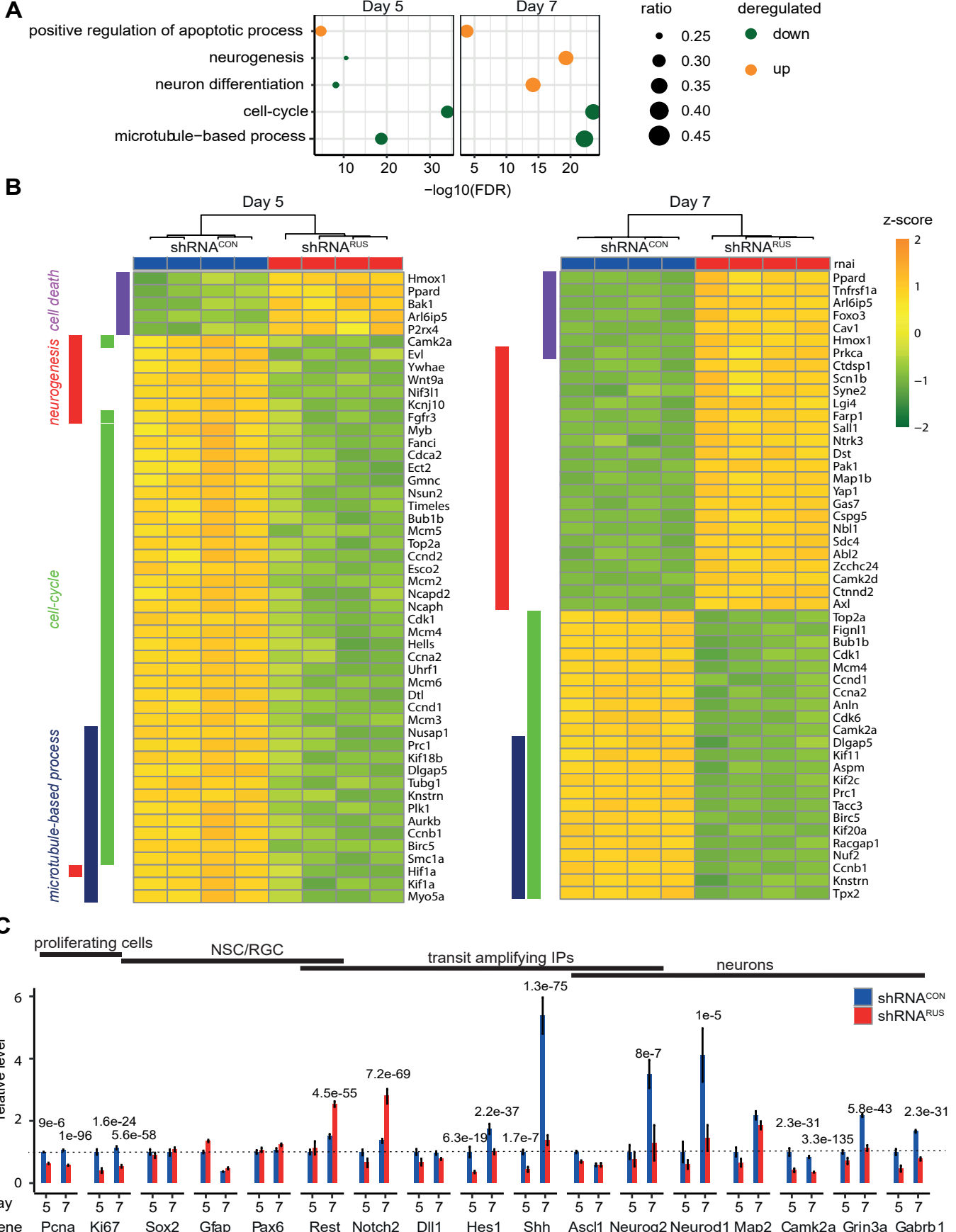
A
positive regulation of apoptotic process
neurogenesis
neuron differentiation
cell-cycle
microtubule−based process
Day 5
Day 7
10
20
30
5
10
15
20
−log10(FDR)
ratio
0.25
0.30
0.35
0.40
0.45
deregulated
down
up
B
Day 5
Day 7
shRNA^CON
shRNA^RUS
z-score
2
1
0
−1
−2
neurogenesis
cell death
cell-cycle
microtubule-based process
Hmox1
Ppard
Bak1
Arl6ip5
P2rx4
Camk2a
Evl
Ywhae
Wnt9a
Nif3l1
Kcnj10
Fgfr3
Myb
Fanci
Cdca2
Ect2
Gmnc
Nsun2
Timeles
Bub1b
Mcm5
Top2a
Ccnd2
Esco2
Mcm2
Ncapd2
Ncaph
Cdk1
Mcm4
Hells
Ccna2
Uhrf1
Mcm6
Dtl
Ccnd1
Mcm3
Nusap1
Prc1
Kif18b
Dlgap5
Tubg1
Knstrn
Plk1
Aurkb
Ccnb1
Birc5
Smc1a
Hif1a
Kif1a
Myo5a
rnai
Ppard
Tnfrsf1a
Arl6ip5
Foxo3
Cav1
Hmox1
Prkca
Ctdsp1
Scn1b
Syne2
Lgi4
Farp1
Sall1
Ntrk3
Dst
Pak1
Map1b
Yap1
Gas7
Cspg5
Nbl1
Sdc4
Abl2
Zcchc24
Camk2d
Ctnnd2
Axl
Top2a
Fignl1
Bub1b
Cdk1
Mcm4
Ccnd1
Ccna2
Anln
Cdk6
Camk2a
Dlgap5
Kif11
Aspm
Kif2c
Prc1
Tacc3
Birc5
Kif20a
Racgap1
Nuf2
Ccnb1
Knstrn
Tpx2
C
proliferating cells
NSC/RGC
transit amplifying IPs
neurons
shRNA^CON
shRNA^RUS
relative level
0
2
4
6
9e-6
1e-96
1.6e-24
5.6e-58
4.5e-55
7.2e-69
6.3e-19
2.2e-37
1.7e-7
1.3e-75
8e-7
1e-5
2.3e-31
3.3e-135
5.8e-43
2.3e-31
Day
5 7
Gene
Pcna
Ki67
Sox2
Gfap
Pax6
Rest
Notch2
Dll1
Hes1
Shh
Ascl1
Neurog2
Neurod1
Map2
Camk2a
Grin3a
Gabrb1

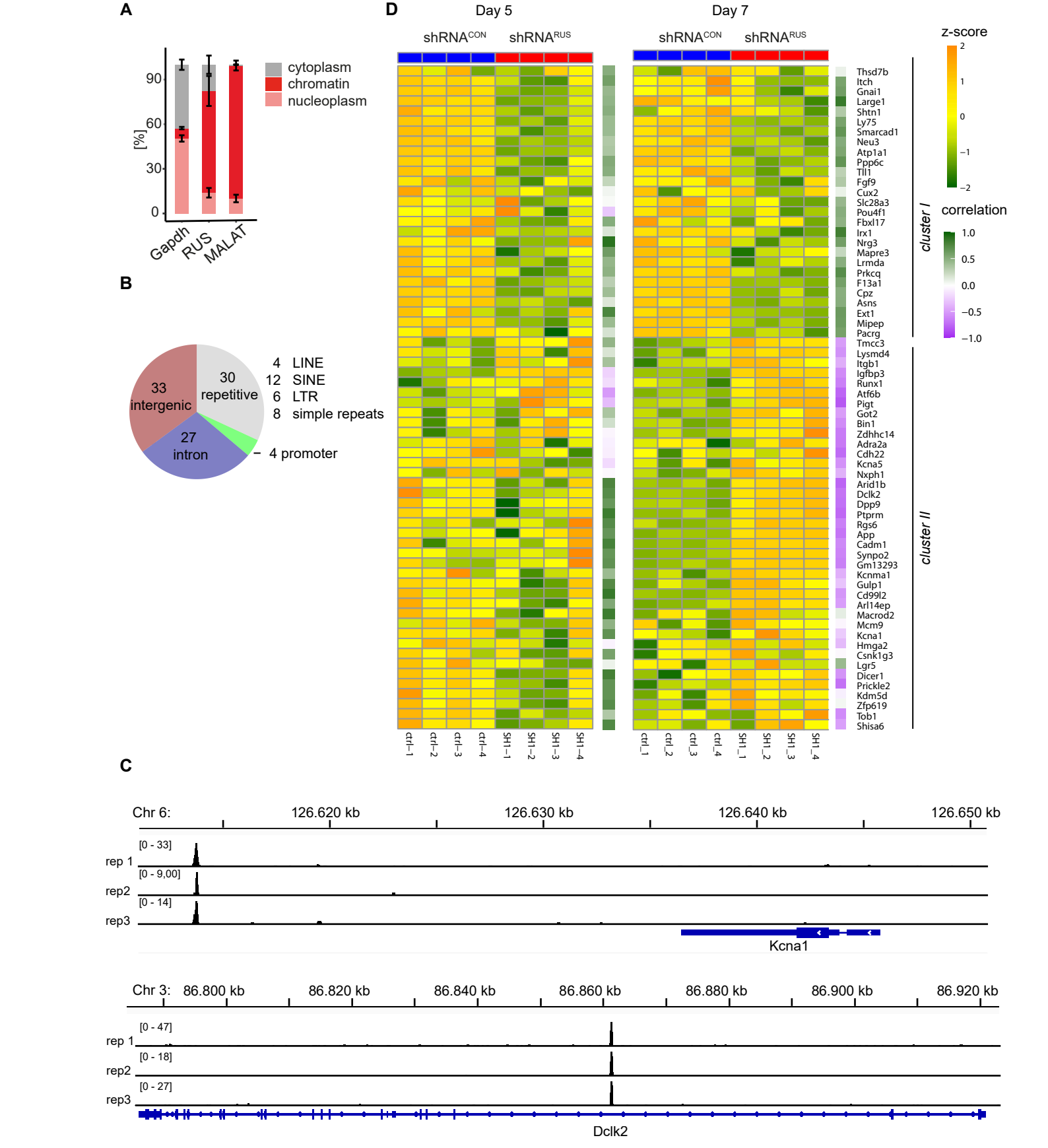
A
cytoplasm
chromatin
nucleoplasm
[%]
90
60
30
0
Gapdh
RUS
MALAT
B
33
intergenic
30
repetitive
27
intron
4 promoter
4 LINE
12 SINE
6 LTR
8 simple repeats
D
Day 5
Day 7
shRNA^CON
shRNA^RUS
z-score
2
1
0
−1
−2
correlation
1.0
0.5
0.0
−0.5
−1.0
cluster I
cluster II
Thsd7b
Itch
Gnai1
Large1
Shtn1
Ly75
Smarcad1
Neu3
Atp1a1
Ppp6c
Tll1
Fgf9
Cux2
Slc28a3
Pou4f1
Fbxl17
Irx1
Nrg3
Mapre3
Lrmda
Prkcq
F13a1
Cpz
Asns
Ext1
Mipep
Pacrg
Tmcc3
Lysmd4
Itgb1
Igfbp3
Runx1
Atf6b
Pigt
Got2
Bin1
Zdhhc14
Adra2a
Cdh22
Kcna5
Nxph1
Arid1b
Dclk2
Dpp9
Ptprm
Rgs6
App
Cadm1
Synpo2
Gm13293
Kcnma1
Gulp1
Cd99l2
Arl14ep
Macrod2
Mcm9
Kcna1
Hmga2
Csnk1g3
Lgr5
Dicer1
Prickle2
Kdm5d
Zfp619
Tob1
Shisa6
ctrl−1
ctrl−2
ctrl−3
ctrl−4
SH1−1
SH1−2
SH1−3
SH1−4
ctrl_1
ctrl_2
ctrl_3
ctrl_4
SH1_1
SH1_2
SH1_3
SH1_4
C
Chr 6:
126.620 kb
126.630 kb
126.640 kb
126.650 kb
rep 1
[0 - 33]
rep2
[0 - 9,00]
rep3
[0 - 14]
Kcna1
Chr 3:
86.800 kb
86.820 kb
86.840 kb
86.860 kb
86.880 kb
86.900 kb
86.920 kb
rep 1
[0 - 47]
rep2
[0 - 18]
rep3
[0 - 27]
Dclk2

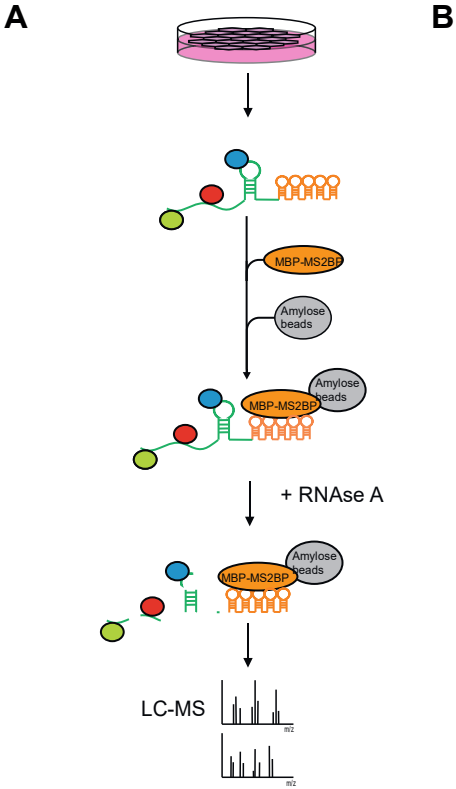
A
MBP-MS2BP
Amylose beads
+ RNAse A
LC-MS

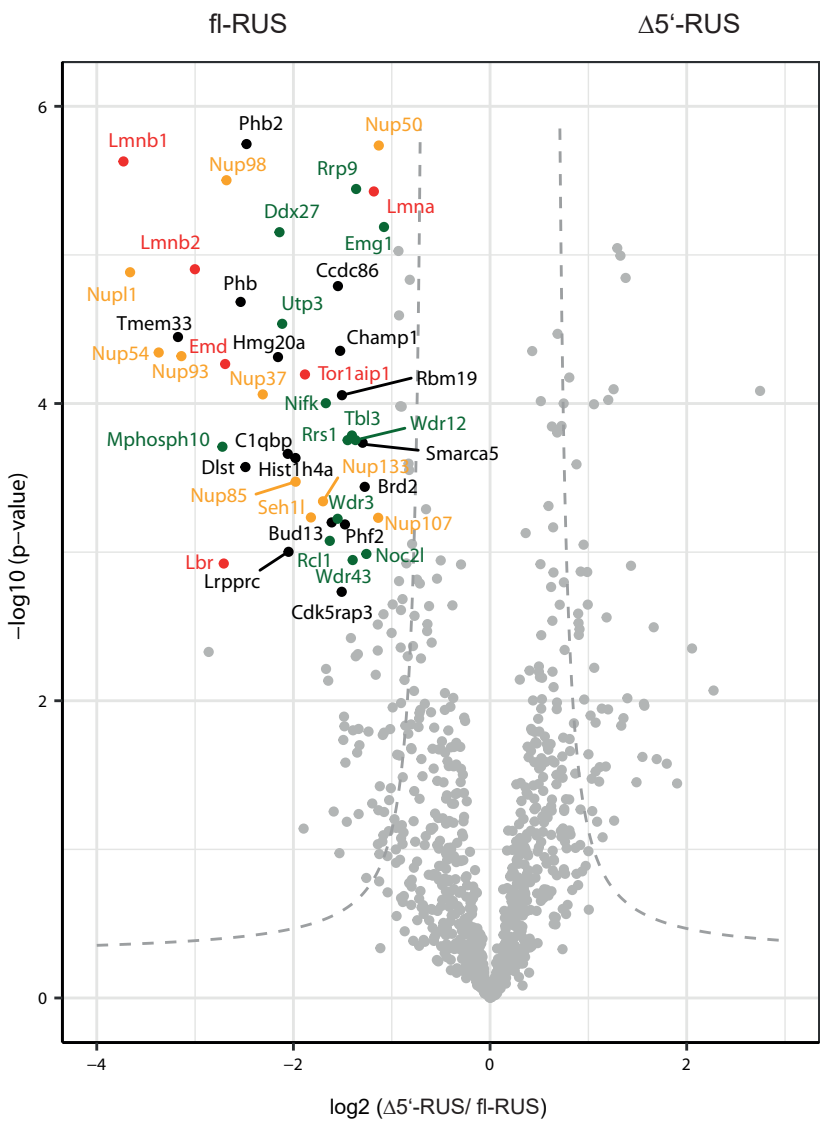
B
fl-RUS
Δ5'-RUS
−log10 (p−value)
log2 (Δ5'-RUS/ fl-RUS)
Lmnb1
Phb2
Nup50
Nup98
Rrp9
Lmna
Ddx27
Lmnb2
Emg1
Ccdc86
Nupl1
Phb
Utp3
Tmem33
Champ1
Nup54
Emd
Hmg20a
Nup93
Nup37
Tor1aip1
Rbm19
Nifk
Tbl3
Wdr12
Mphosph10
C1qbp
Rrs1
Smarca5
Dlst
Hist1h4a
Nup133
Brd2
Nup85
Seh1l
Wdr3
Nup107
Bud13
Phf2
Lbr
Rcl1
Noc2l
Lrpprc
Wdr43
Cdk5rap3

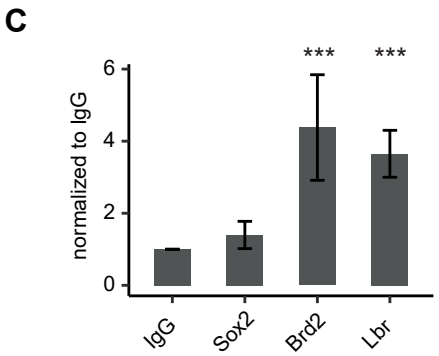
C
normalized to IgG
***
***
IgG
Sox2
Brd2
Lbr

A

```
    *          *          *          *          *          *
118 ACTTCATTTATGTTAAAATCAACAATATTATTCATATTAAAAACATATGCTCTATAGCTCCC~~~~~~~~~~~ annotated lncRNA
    ||||||||||||||||||||||#||||||||||||||||||||||||||||||||||##|||||
701 ACTTCATTTATGTTAAAATCATCAATATTATTCATATTAAAAACATATGCTCTATNNCTCCCCGAAAAAAAAA Sanger sequencing result
          *          *          *          *          *          *          *
```

annotated 3‘ end — 3‘RACE adaptor

B

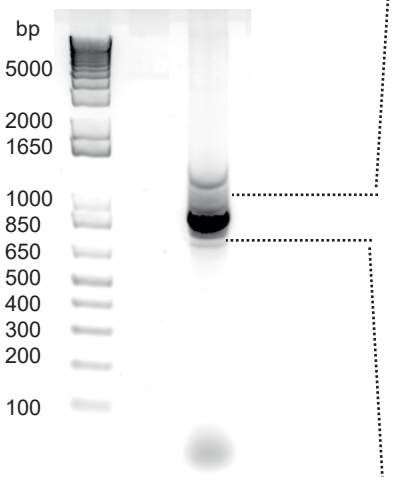


```
   1 AGAGCATTTGGGCTTAAGCCGGTTCAGCTCAGAGGTGGGTTTCGGAAGTCTGTGGCGGAC 60
     exon 1
  61 CACCGCAGCAAGTCATCACTCAGCGTACAAGCCTTTCCATTTCTGAAAATATAAAGAACT 120

 121 TAAGCATGCGGCGTTCGGAGTGTAGATTGCTTTGAGGTATTTCAAAGCAGCGCTGATCAT 180

 181 GGGCAGAGGAGCTGATATGTGCAACAGAAACTACTCACTGGAACTCTTCTGGACGTCTGT 240
                                                        exon 2
 241 CCTCTGTAATGCAAGTGTCTGCCCTCACTCTGGCGACTGTGCTGTTGGAACGCTGGTGCT 300

 301 CATCTTTCACTGTCCTCCACAAAGCATGCCTCAGGACTGTAGGCAGCCTGTTTATGCCAT 360
                                                   exon 3
 361 TGTAAGACTACCCCTGGGAAGGAGGGACAGACCTAAAAAATTCACTAACAATTCTGACTA 420

 421 AACTGACCTGTCTCCTAACATAGAGAAGATTGGCAGCCAGAAAGACCTGGATATCCCACC 480
         exon 5
 481 TCCATTGCCCACTGCACTGTGGTTACAGCATGAAGCCATAACTGGCTCTTTAGTTCTATG 540

 541 CCATGAAATTCAACTCTCATTTTCATGCTTGTGCACTAATCCTAAAAGTATCATATTCCC 600

 601 AAATGGTTATTTTGTTTTCTGTATTTGCAAATACTTGTTTTCTTTTCTTAATGGAGTTTG 660

 661 TAGGCCCATAAGTTACTTCTACTCAATTTTATCATTTCGATATGATTCTTTCATGTTCTG 720

 721 AGGATTGGTTGGAAAAAGATCCTAGTCATTAGTGTACAGGTTCCAATCTCAAATATAAAA 780

 781 TCTATACATGGAATCCTTACTAATTTTTTTTTACCTGTATAATTTCTTTACTATGGCTCC 840

 841 TACCACCTTCACTTCATTTATGTTAAAATCAACAATATTATTCATATTAAAAACATATGC 900

 901 TCTATAGCTCCC 912
```

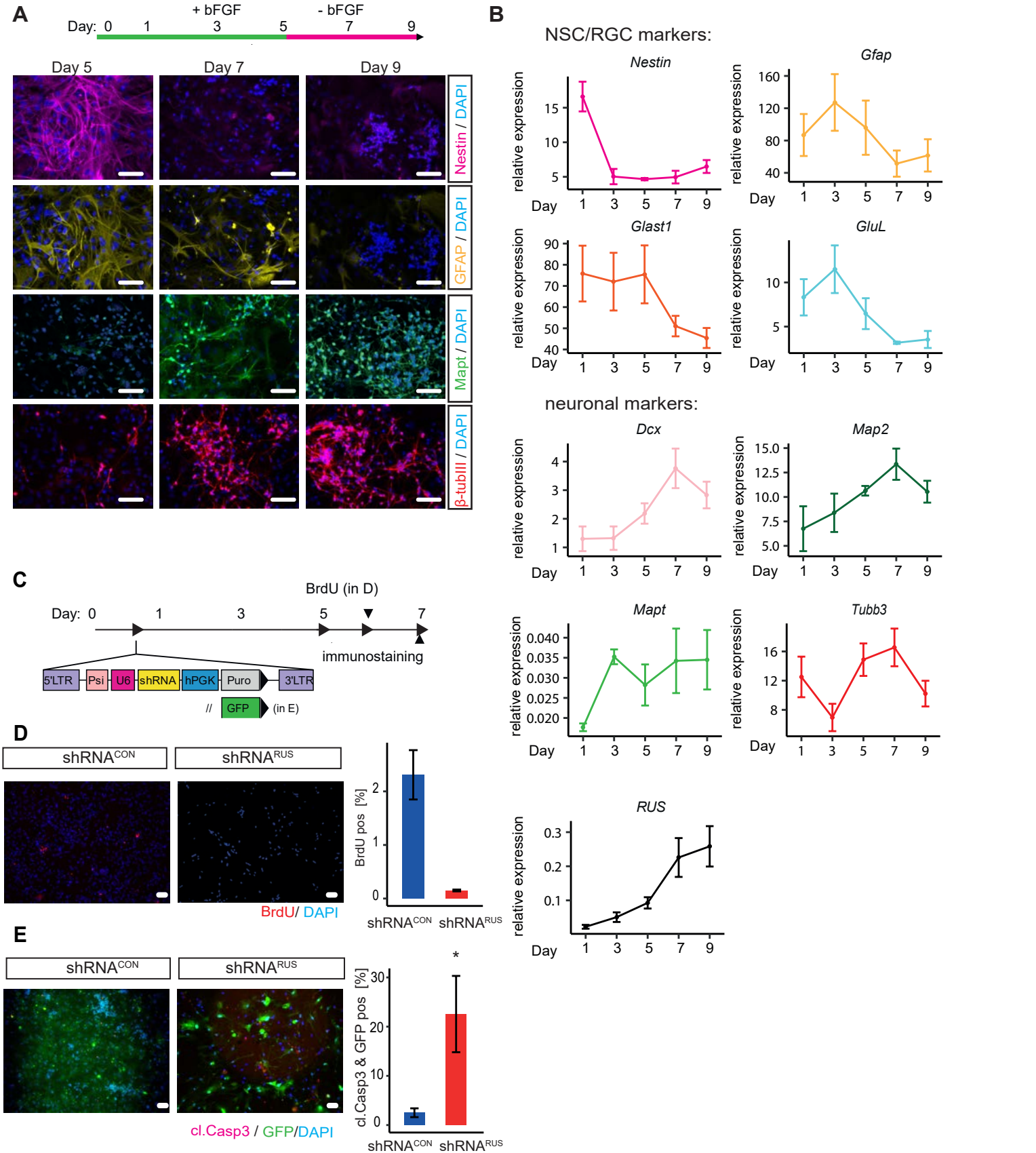
A
+ bFGF
- bFGF
Day: 0 1 3 5 7 9
Day 5
Day 7
Day 9
Nestin / DAPI
GFAP / DAPI
Mapt / DAPI
β-tubIII / DAPI
B
NSC/RGC markers:
Nestin
Gfap
Glast1
GluL
neuronal markers:
Dcx
Map2
Mapt
Tubb3
RUS
relative expression
Day
C
BrdU (in D)
Day: 0 1 3 5 7
immunostaining
5'LTR
Psi
U6
shRNA
hPGK
Puro
3'LTR
GFP
(in E)
D
shRNA^CON
shRNA^RUS
BrdU/ DAPI
BrdU pos [%]
E
cl.Casp3 / GFP/DAPI
cl.Casp3 & GFP pos [%]
*

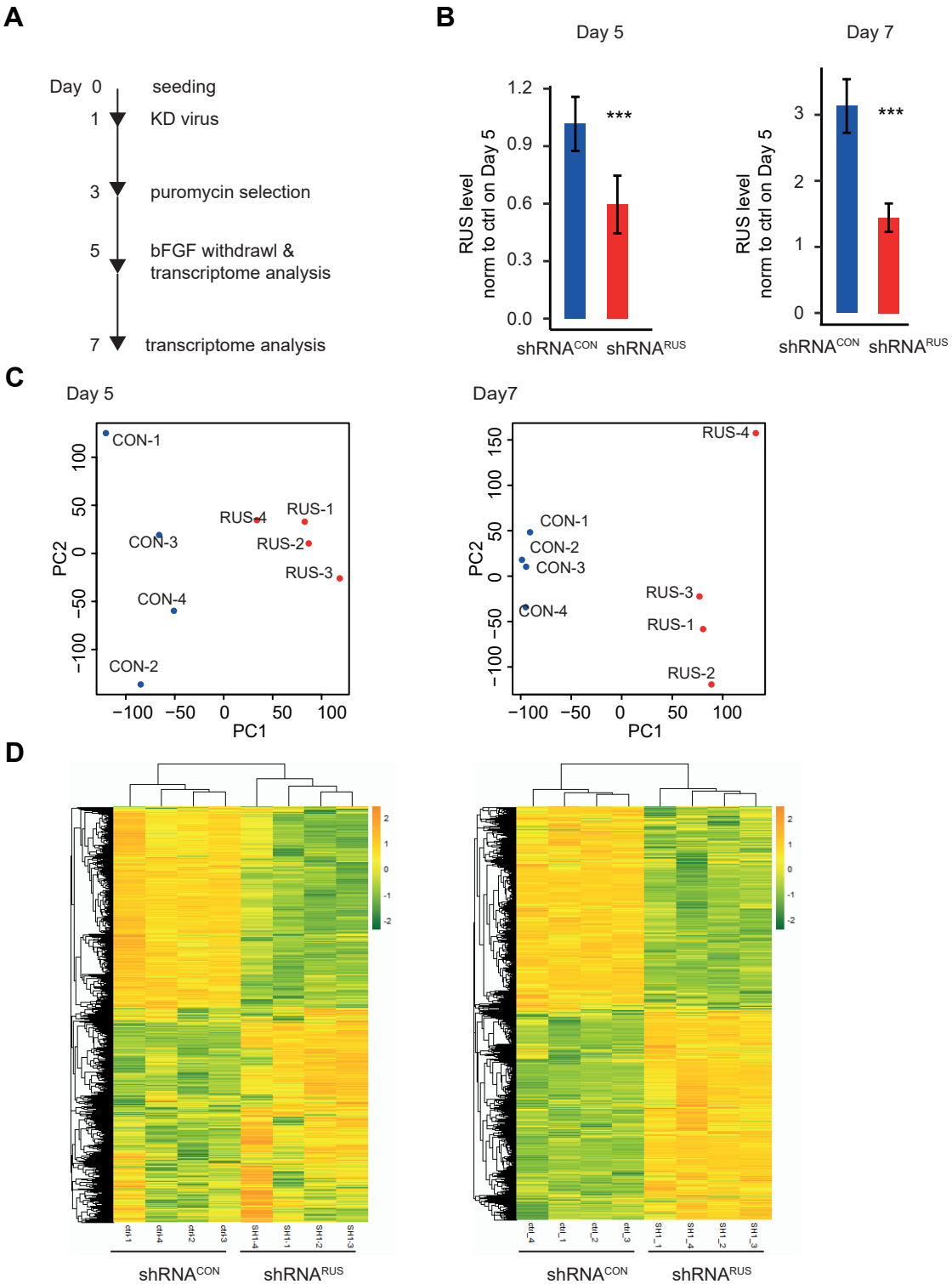
A
Day 0
seeding
1
KD virus
3
puromycin selection
5
bFGF withdrawl &
transcriptome analysis
7
transcriptome analysis
B
Day 5
Day 7
RUS level
norm to ctrl on Day 5
***
shRNA^CON
shRNA^RUS
C
Day 5
Day7
PC1
PC2
CON-1
CON-2
CON-3
CON-4
RUS-1
RUS-2
RUS-3
RUS-4
D
shRNA^CON
shRNA^RUS

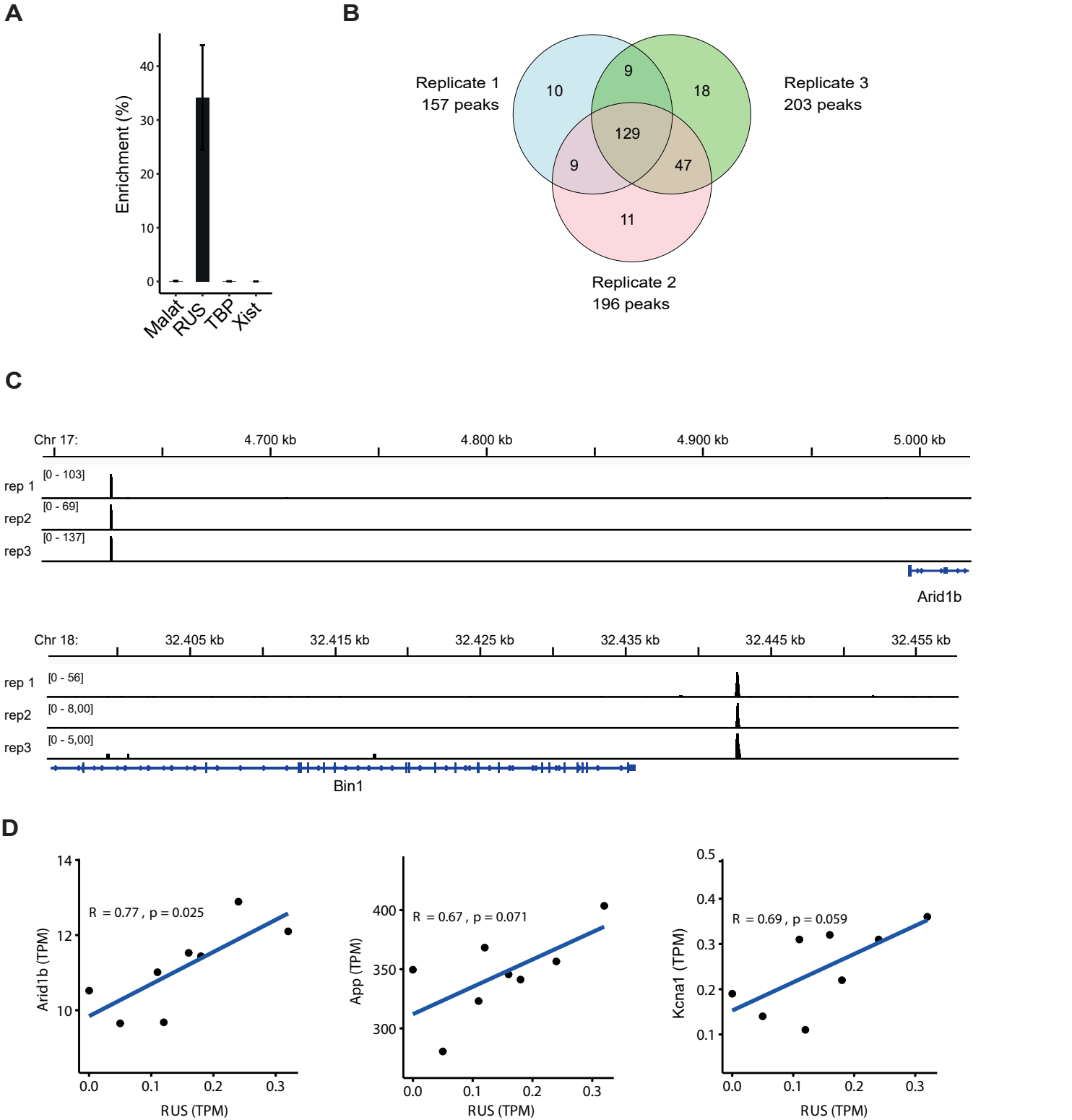
A
Enrichment (%)
40
30
20
10
0
Malat
RUS
TBP
Xist
B
Replicate 1
157 peaks
Replicate 3
203 peaks
Replicate 2
196 peaks
10
9
18
129
9
47
11
C
Chr 17:
4.700 kb
4.800 kb
4.900 kb
5.000 kb
rep 1
[0 - 103]
rep2
[0 - 69]
rep3
[0 - 137]
Arid1b
Chr 18:
32.405 kb
32.415 kb
32.425 kb
32.435 kb
32.445 kb
32.455 kb
rep 1
[0 - 56]
rep2
[0 - 8,00]
rep3
[0 - 5,00]
Bin1
D
Arid1b (TPM)
R = 0.77 , p = 0.025
RUS (TPM)
App (TPM)
R = 0.67 , p = 0.071
RUS (TPM)
Kcna1 (TPM)
R = 0.69 , p = 0.059
RUS (TPM)

UniProt ID	gene name	-LOG10 (p-value)	log2(mut/fl)	only detected by full length *RUS*	nuclear compartment
Q7JJ13	Brd2	3.44	-1.27	no	-
Q8R149	Bud13	3.20	-1.61	no	-
O35658	C1qbp	3.66	-2.06	no	-
Q9JJ89	Ccdc86	4.79	-1.55	no	-
Q99LM2	Cdk5rap3	2.73	-1.51	no	-
Q8K327	Champ1	4.35	-1.52	no	-
Q921N6	Ddx27	5.15	-2.14	no	nucleolus
O08749	Dld	6.00	-2.13	no	-
Q9D2G2	Dlst	3.57	-2.49	no	-
O08579	Emd	4.27	-2.69	no	nuclear lamin
O35130	Emg1	5.19	-1.08	no	nucleolus
P62806	Hist1h4a	3.63	-1.98	no	-
Q9DC33	Hmg20a	4.31	-2.16	no	-
P38647	Hspa9	6.57	-1.99	no	-
Q3U9G9	Lbr	2.92	-2.71	no	nuclear lamin
P48678	Lmna	5.43	-1.18	no	nuclear lamin
P14733	Lmnb1	5.63	-3.73	no	nuclear lamin
P21619	Lmnb2	4.90	-3.00	no	nuclear lamin
Q6PB66	Lrpprc	3.00	-2.05	no	-
Q810V0	Mphosph10	3.71	-2.72	no	nucleolus
Q91VE6	Nifk	4.00	-1.67	no	nucleolus
Q9WV70	Noc2l	2.99	-1.26	no	nucleolus
Q8BH74	Nup107	3.23	-1.14	no	nuclear pore
Q8R0G9	Nup133	3.34	-1.70	no	nuclear pore
Q9CWU9	Nup37	4.06	-2.31	no	nuclear pore
P59235	Nup43	6.28	-2.93	no	nuclear pore
Q9JIH2	Nup50	5.74	-1.13	no	nuclear pore
Q8BTS4	Nup54	4.34	-3.37	no	nuclear pore
Q8R480	Nup85	3.47	-1.98	no	nuclear pore
Q8BJ71	Nup93	4.32	-3.14	no	nuclear pore
Q6PFD9	Nup98	5.50	-2.68	no	nuclear pore
Q8R332	Nupl1	4.88	-3.66	no	nuclear pore
P67778	Phb	4.68	-2.54	yes	-
O35129	Phb2	5.75	-2.48	yes	-
Q9WTU0	Phf2	3.19	-1.48	no	-
Q8R3C6	Rbm19	4.06	-1.51	no	-
Q9JJT0	Rcl1	3.08	-1.63	no	nucleolus
Q91WM3	Rrp9	5.44	-1.36	no	nucleolus
Q9CYH6	Rrs1	3.75	-1.45	no	nucleolus
Q8R2U0	Seh1l	3.23	-1.82	no	nuclear pore
Q91ZW3	Smarca5	3.74	-1.30	no	-
Q8C4J7	Tbl3	3.78	-1.41	no	nucleolus
Q9CR67	Tmem33	4.45	-3.17	no	-
Q921T2	Tor1aip1	4.20	-1.88	yes	nuclear lamin
Q9JI13	Utp3	4.54	-2.11	yes	nucleolus
Q9JJA4	Wdr12	3.75	-1.37	no	nucleolus
Q8BHB4	Wdr3	3.22	-1.55	no	nucleolus
Q6ZQL4	Wdr43	2.95	-1.40	no	nucleolus

Structured Methods

Reagents and Tools Table

Reagent/Resource	Reference or Source	Identifier or Catalog Number
Experimental Models		
C57BL/6J (M. musculus)	Jackson Lab	NA
Dh5α	NEB	C 29871
Hek 293T	LGC standards	ATCC® CRL-11268™
Neuro-2a	LGC standards	ATCC® CCL-131™
Neuro-2a FRT	this study	NA
Neuro-2a - full-length RUS	this study	NA
Neuro-2a-$\Delta_{5'RUS}$	this study	NA
Recombinant DNA		
pLKO-TRC-Puro	Addgene	#10878
pLKO-scr-Puro	Addgene	#1864
pLKO-shRUS-Puro	this study	NA
pLKO-scr-GFP	this study	NA
pLKO-shRUS-GFP	this study	NA
pMD2.G	Addgene	#12259
psPAX2	Addgene	#12260
pAdMl3-(MS2)3	gifted	NA
pcDNA5-FRT	Thermo Fischer	V601020
pcDNA5-FRT-5xMS2	this study	NA
pcDNA5-FRT-RUS	this study	NA
pcDNA5-FRT-RUS-5xMS2	this study	NA
pcDNA5-FRT-5'ΔRUS-5xMS2	this study	NA
pLenti-CMV-GFP-Hygro	Addgene	#17446
pLenti-CMV-GFP-Puro	Addgene	#17448
pLenti-RUS	this study	NA
pLenti-FRT	this study	NA
pCSFLPe	addgene	#31130
Antibodies		
Donkey DyLight550-αIgG-mouse	Thermo Fischer	SA5-10167
Donkey DyLight550-αIgG-rabbit	Thermo Fischer	SA5-10039

Donkey DyLigth488-αIgG-mouse	Thermo Fischer	SA5-10166
Donkey DyLigth488-αIgG-rabbit	Thermo Fischer	SA5-10038
Goat Gfap	Santa Cruz	sc-6170
Rabbit Glast1	Thermo Fischer	# PA5-80012
Mouse β-tubulin III	Covance	MMS-435P
Mouse BrdU	BioRad	MCA2483GA
Mouse Map2	Abcam	#11267
Rabbit caspase3 (Asp175)	cell signalling	#9664
Mouse Sox2	Thermo Fischer	MA1-014
Rabbit IgG	cell signaling	#2729
Rabbit Lbr	abcam	ab122919
Oligonucleotides and other sequence-based reagents		
shRNAs	This study	Table EV1
PCR primers	This study	Table EV1
RUS probes	LGC	Table EV1
Chemicals, Enzymes and other reagents		
DNAse (RNAse free)	roche / sigma aldrich	4716728001
Fast SYBR® Green Master Mix	Thermo Fischer	4385614
M-MLV Reverse Transcriptase	Thermo Fischer	28025013
murine RNAse Inhibitor	NEB	M0314L
Phusion Hf-DNA Polymerase	NEB	M0530L
Proteinase K (RNAse free)	Thermo Fischer	AM2548
RNase A, DNase and protease-free	Thermo Fischer	EN0531
RNAse H	NEB	M0297L
T4 DNA Ligase	NEB	M0202L
T4 DNA Polymerase	NEB	M0203S
Protein A Agarose	Millipore	16-125
Protein G Agarose	Millipore	16-266
Amylose resin	NEB	E 8021S
AMPure XP	Beckan Coulter	A63881
FirstChoice™ RLM-RACE Kit	Thermo Fischer	AM1700M

Pierce™ Protein A/G Magnetic Beads	Thermo Fischer	88802
Dynabeads™ MyOne™ Streptavidin C1	Thermo Fischer	65001
NEBNext® Ultra™ II DNA Library Prep with Sample Purification Beads	NEB	E7103L
NEBNext® Multiplex Oligos for Illumina®	NEB	E6440S
AflII	NEB	R 0520L
Age I, recombinant	NEB	R 0552 S
Age I-HF	NEB	R 3552 S
ApaI	NEB	R0114S
BamH I-HF	NEB	R 3136 S
EcoR I-HF	NEB	R 3101 S
KpnI-HF	NEB	R3142 L
B-27® Supplement (50X), serum free	Thermo Fischer	17504001
DMEM, high glucose, GlutaMAX™ Supplement	Thermo Fischer	61965-059
DMEM/F12	Thermo Fischer	11330-057
FCS	PAN Biotech	P40-37 500
Neurobasal medium	Thermo Fischer	21103-049
poly-D-Lysine HBr	Sigma-Aldrich	P7280
Recombinant Human FGF-basic (154 a.a.)	peprotech	100-18B
Trypsin-EDTA (0.05%), phenol red	Thermo Fischer	25300-062
GlutaMAX™ Supplement	Thermo Fischer	35050038
Trypsin	Promega	Cat#V5111
LysC	Promega	Cat#V1671
ReproSil-Pur 120 C18-AQ, 1.9 µm	Dr. Maisch GmbH	Cat#r119.aq.
Software		
Ape - plasmid editor	https://jorgensen.biology.utah.edu/wayned/ape/	
ImageJ	https://imagej.nih.gov/ij/index.html	
python 2.7	https://www.python.org/download/releases/2.7/	
annaconda	https://docs.anaconda.com/	
bowtie 2	http://bowtie-bio.sourceforge.net/bowtie2/index.shtml	
	(Langmead & Salzberg, 2012)	

Star 2.0	https://github.com/alexdobin/STAR/releases	
	(Dobin, et al., 2012)	
Rsem	https://github.com/deweylab/RSEM	
	(Li & Dewey, 2011)	
samtools	http://www.htslib.org/doc/samtools-index.html	
	(Li, et al., 2009)	
deeptools	https://deeptools.readthedocs.io/en/develop/	
	(Ramirez, et al., 2016)	
bedtools	https://bedtools.readthedocs.io/en/latest/	
	(Quinlan & Hall, 2010)	
MACS1.4	https://github.com/liulab-dfci/MACS	
	(Feng, et al., 2011)	
Meme Suit	https://meme-suite.org/meme/	
	(Bailey, et al., 2015)	
Homer	http://homer.ucsd.edu/homer/	
	(Heinz, et al., 2010)	
PANTHER	http://geneontology.org/docs/go-enrichment-analysis/	
	(Mi , et al., 2013)	
MaxQuant (version 1.5.5.1 or 1.6.1.0)	https://www.maxquant.org/	
	(Cox & Mann., 2008)	
Perseus (version 2.0.3)	https://www.maxquant.org/	
	(Tyanova, et al., 2016)	
R 4.0.2	https://www.r-project.org/about.html	
Rstudio	https://www.rstudio.com/	
rmarkdown	https://rmarkdown.rstudio.com/	
Biocoductor	https://bioconductor.org/	
dplyr	https://dplyr.tidyverse.org/	
magrittr	https://magrittr.tidyverse.org/	
knitr	https://www.r-project.org/nosvn/pandoc/knitr.html	

ggplot	https://ggplot2.tidyverse.org/	
biomaRt	https://m.ensembl.org/info/data/biomart/index.html	
	(Smedley, et al., 2009)	
DESeq2	https://bioconductor.org/packages/release/bioc/html/DESeq2.html	
	(Love, et al., 2014)	
SummarizedExperiments	https://bioconductor.org/packages/release/bioc/html/SummarizedExperiment.html	
SummaryTools	https://cran.r-project.org/web/packages/summarytools/index.html	
GenomicRanges	https://bioconductor.org/packages/release/bioc/html/GenomicRanges.html	
	(Lawrence, et al., 2013)	
Rsubread	https://bioconductor.org/packages/release/bioc/html/Rsubread.html	
	(Liao, et al., 2019)	
takeLower.py	https://github.com/bdo311/chirpseq-analysis/blob/master/takeLower.py	
Other		
Illumina NexSeq 500	Illumina	
Q Exactive™ HF Hybrid Quadrupol-Orbitrap™ mass spectrometer	Thermo Fisher Scientific	IQLAAEGAAPFALGMBFZ
real time pcr detection system, 384 wells	Biorad	CFX384
Mastercycler nexus gradient	Eppendorf	6331000017
STEPONE PLUS 96-well RT PCR SYS	Thermo Fischer	4376599